Interference mitigation in GNSS signal acquisition through antenna arrays

Dr. Javier Arribas

Centre Tecnològic de Telecomunicacions de Catalunya (CTTC)

Interference Management for Tomorrow's Wireless Networks
Newcom# Summer School Sophia Antipolis - May 28-31, 2013

Overview

Introduction to GNSS

- Global Navigation Satellite Systems (GNSS) is *the general concept used to identify those positioning systems that enable the determination of the user position and time by means of measured distances between the receiver and a set of visible satellites.*

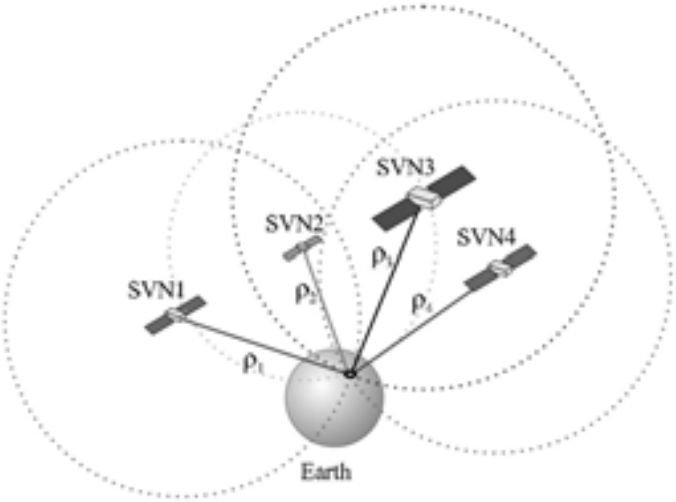

Figure: Position determination by GNSSs. Source: Kai Borre, Darius Plausinaitis, Reconfigurable GNSS Receivers, 2007.

(a) GPS (b) Galileo (c) Glonass (d) Compass (e) IRNSS (f) QZSS

GNSS signal structure

DS-CDMA transmitted signal for the i-th satellite:

$$s_{T,i}(t) = e_{I,i}(t) + je_{Q,i}(t), \tag{1}$$

where the subindex I and Q denote in-phase and quadrature component respectively, and are defined as:

$$e_{I,i}(t) = \sqrt{2P_{I,i}} \sum_{m_I=-\infty}^{\infty} b_{I,i}(m_I) \sum_{u_I=1}^{N_{c_I}} \sum_{k_I=1}^{L_{c_I}} c_{I,i}(k_I) g_I(t - m_I T_{b_I} - u_I T_{PRN_I} - k_I T_{c_I}) \tag{2}$$

with the following definitions for the I component - analogous for the Q component:

- $P_{I,i}$ is the transmitted signal power.
- $b_{I,i}(m) \in \{-1, 1\}$ is the sequence of telemetry bits, with T_{b_I} being the bit period.
- $c_{I,i}(k) \in \{-1, 1\}$ is the Pseudo Random Noise (PRN) spreading sequence, with the chip length of the codeword and the chip period defined as L_{c_I} and T_{c_I}, respectively. $T_{PRN_I} = L_{c_I} T_{c_I}$ is the codeword period. The number of code epochs per telemetry bit is N_{c_I}.
- $g_I(t)$ is the energy-normalized chip shaping pulse.

Simplified receiver signal model

Considering only the LOSS contribution coming from M_s satellites and the predominant propagation effects:

$$x_{RF}(t) = \Re\left\{\sum_{i=1}^{M_s} \alpha_i(t) s_{T,i}(t-\tau_i(t)) e^{j2\pi(f_c+f_{d,i}(t))t}\right\} + n(t), \tag{3}$$

where f_c is the carrier frequency, $\boldsymbol{\theta}_i = [\alpha_i(t), f_{d,i}(t), \tau_i(t)]$ are the complex amplitude, the Doppler frequency shift, and the time delay, respectively, which are the signal synchronization parameters for the i-th satellite signal and $n(t)$ is additive white **Gaussian noise plus other undesired terms (such as multipath or interferences)**. The implicit channel model is defined as Wide-Sense Stationary Uncorrelated Scattering (WSSUS).

GNSS receiver block diagram

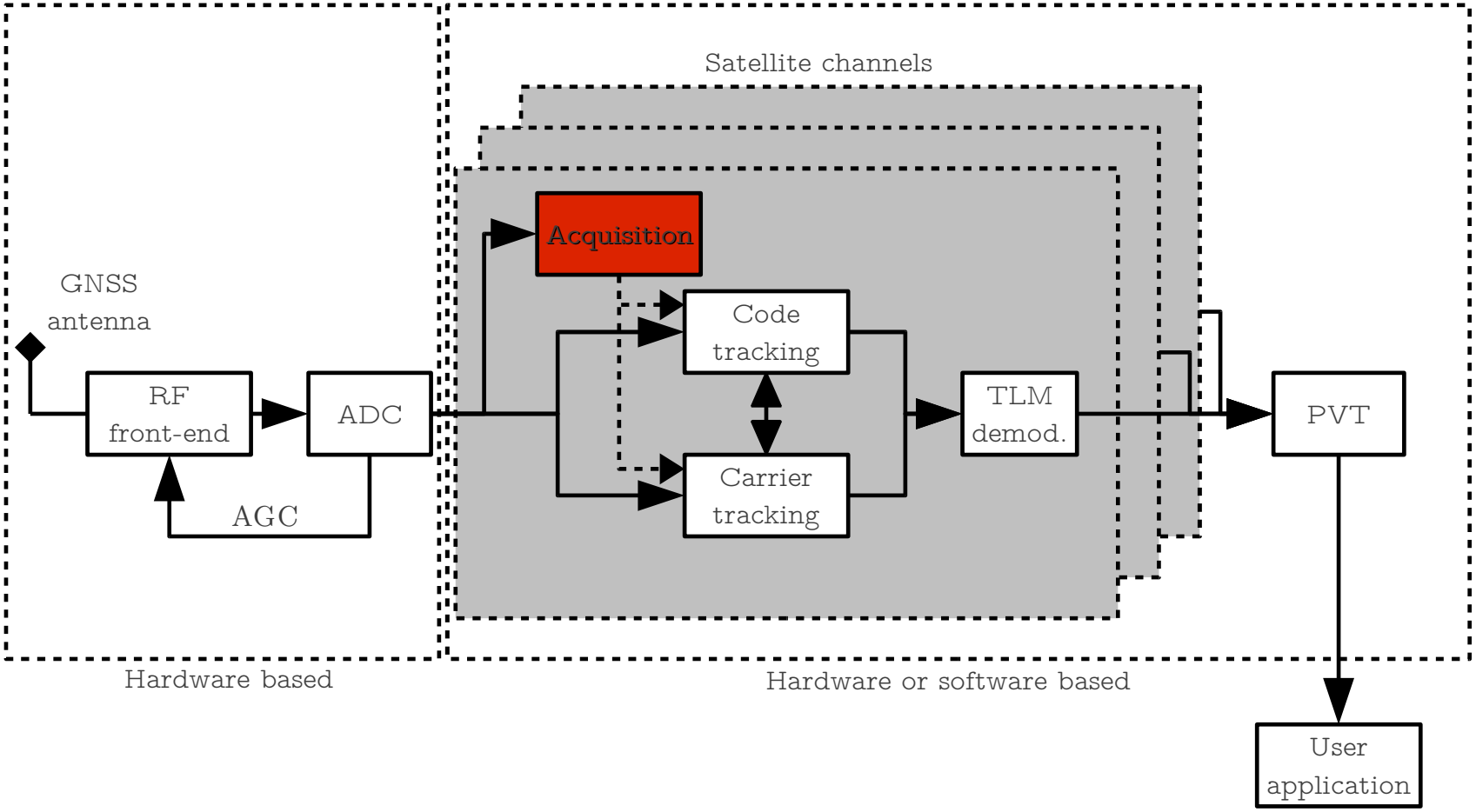

Figure: Simplified GNSS receiver high-level block diagram.

Acquisition operation

Target: provide a coarse estimation of the synchronization parameters vector $\boldsymbol{\theta}_i$ for each received satellite:

$$\hat{\boldsymbol{\theta}}_i = [\hat{\alpha}_i, \quad \underbrace{\hat{f}_{d,i}, \hat{\tau}_i}_{\text{Grid Search}} \quad] \tag{4}$$

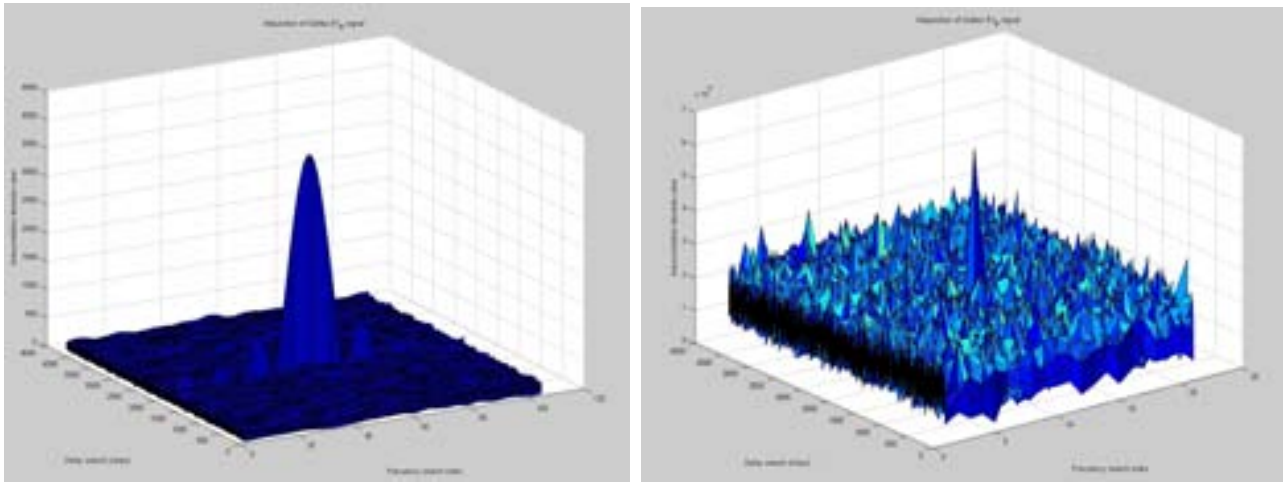

Figure: Acquisition test function output vs. time-delay and Doppler-shift of a noise-free and noisy Galileo-like MBOC(6,1,1/11) signal.

Acquisition parameters

Acquisition performance indicators

- Sensitivity
- $TTFF_{cold} = T_{warm-up} + T_{acq} + T_{track} + T_{NAV+GST} + T_{PVT}$

Performance degradation sources:

- Signal attenuation: fading and low level signal conditions.
- **Interferences**.
- Navigation message.
- Receiver and satellite movement.
- Receiver sample clock drift.

GNSS Interference sources

Among the **VHF and UHF spurious transmissions** (DVB-T, TACAN, and DME), the adjacent frequencies to GNSS links are populated as:

Band [MHz]	Usage
1435-1530	Mobile (aeronautical telemetry)
1530-1545	Mobile-satellite (space-to-Earth) Maritime mobile-satellite (space-to-Earth)
1545-1549.5	Aeronautical mobile-satellite (space-to-Earth) Mobile-satellite (space-to-Earth)
1549.5-1558.5	Aeronautical mobile-satellite (space-to-Earth) Mobile-satellite (space-to-Earth)
1613.8-1626.5	Mobile-satellite (Earth-to-space)
1626.5-1645.5	Mobile-satellite (Earth-to-space)
1646.5-1651	Aeronautical mobile-satellite (Earth-to-space)
1651-1660	Mobile-satellite (Earth-to-space)
1668-1675	Meteorological aids (radiosonde)
1700-1710	Meteorological-satellite (space-to-Earth)
1710-1755	Mobile communications

Table: Sources and Services of image Interference for single-conversion GPS L1 / Galileo E1 front-end [Wil02].

The proposed deployment of Lightsquared's 4G communication network could create a new interference situation specially when using the 1552.7 MHz band, as notified for the first time by the U.S. NTIA to U.S. FCC in January 2011.

Problem definition

- New and upgraded GNSSs are being used to provide **safety-critical guidance**:
  - Modernized GPS and forthcoming Galileo will provide integrity monitoring mechanisms: RAIM, SBAS, GBAS, and Galileo embedded integrity concept.
  - Robust and highly **accurate positioning and time dissemination** service.
  - Used for the transport **safety of persons and goods**, such as in Civil aviation, Railroad transport, and Commercial maritime.

$\Rightarrow$ The acquisition operation can become the bottleneck of GNSS receivers:
  - **Tracking initialization depends on acquisition results**.
  - **Acquisition has the lowest sensitivity of the whole receiver operation**.
  - Strong **interferences and jamming signals** could increase the acquisition time or even can make the acquisition fail.

State-of-the-Art

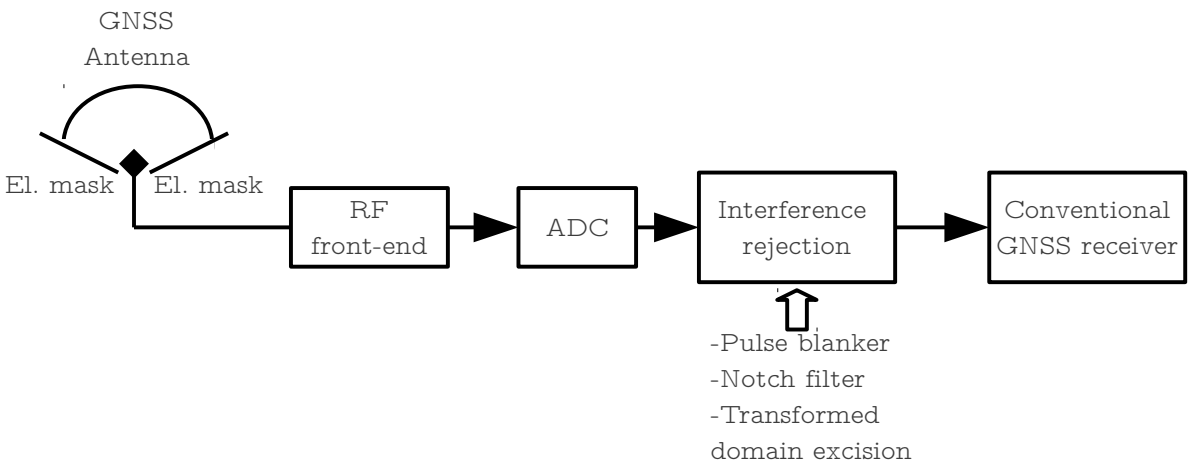

Figure: Single-antenna receiver interference rejection.

Single-antenna solutions for acquisition interference mitigation

- **Time diversity**: pulse blanking and Automatic Gain Control (AGC).
- **Frequency diversity**: Continuous Wave Interference (CWI) notch filters.
- *Spatial diversity*: antenna radiation pattern.

Research opportunity

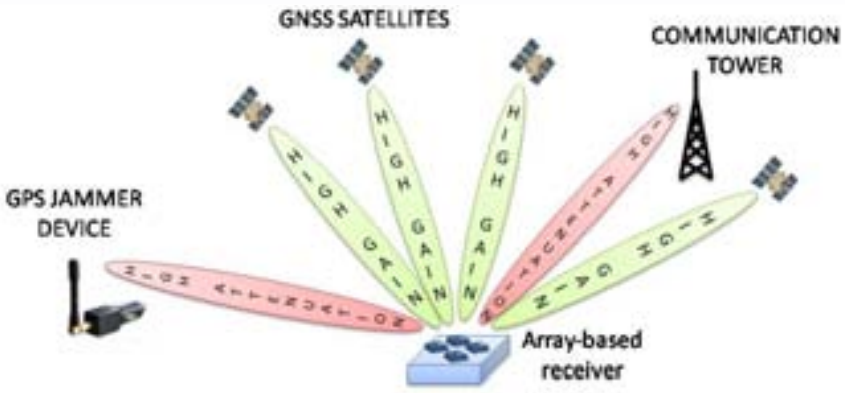

Figure: Array-based GNSS receiver.

- **Antenna-array key benefits**:
  - In addition to code, time and frequency diversities, arrays **exploit spatial diversity**.
  - **Interference and jamming** signals **rejection**.
  - **Sensitivity improvement** due to the array gain.
- **Acquisition with antenna arrays has not yet received much attention**:
  - Intense research activity on single antenna receivers.
  - Antenna arrays applied to tracking **assuming the success of the acquisition**.

⇒ **Existing antenna-array solutions suitable for acquisition**:
  - *Minimum Variance Distortionless Response (MVDR) beamformer*: **requires an estimation of both the signal DOA and the array attitude**.
  - *Spatial-domain grid search*: **requires a calibrated array**, but it increases the dimensions of the search grid.
  - *Blind null-steering beamformers*: **DOA not necessary**, but **no array gain**.

Research opportunity

- **Lack of suitable array-based GNSS real-time receiver commercially available**
  - Closed implementations with **few technical information made public**.

Figure: NovAtel GAJT commercial null-steering GNSS array.

- **Scientific applications of GNSSs require flexible implementations**
  - The **Software Defined Radio (SDR) receiver approach** is suitable to test new algorithms with low development costs.
  - Interest for a limited-market but highly demanding applications such as reference stations, geodesy and surveying, among other scientific goals.

Main objectives of the project

Exploit the spatial diversity in acquisition

- Improve the existing GNSS acquisition algorithms performance.
- **Improve the GNSS interference robustness** proposing **novel array-based acquisition algorithms** using the **statistical detection theory** framework.

Demonstrate the implementation feasibility

- Design and implementation of an array-based GNSS receiver platform
- **Proof-of-concept of array-based acquisition** algorithms working in **real-time**
  - **Interference mitigation**.
  - Performance measurements in **realistic scenarios**.
- Tightly coupled with GNSS software receivers.

Objectives

Exploit the spatial diversity in acquisition

- Improve the existing GNSS acquisition algorithms performance.
- **Improve the GNSS interference robustness** proposing **novel array-based acquisition algorithms** using the **statistical detection theory** framework.

Demonstrate the implementation feasibility

- Design and implementation of an array-based GNSS receiver platform
- **Proof-of-concept** of array-based acquisition algorithms working in **real-time**
  - **Interference mitigation**.
  - Performance measurements in **realistic scenarios**.
- Tightly coupled with GNSS software receivers.

Antenna-array signal model

N-elements baseband array signal model for single satellite:

$$\mathbf{X}(t) = \mathbf{hd}(t, f_d, \tau) + \mathbf{N}(t), \tag{5}$$

where

- $\mathbf{X}(t) = [\mathbf{x}_{bb}(t-(K-1)T_s)\ldots\mathbf{x}_{bb}(t)] \in \mathbb{C}^{N\times K}$ is referred as the *space-time data matrix*, where $\mathbf{x}_{bb}(t) = [x_1(t)\ldots x_N(t)]^T$ is defined as the baseband snapshot, and K is the number of captured snapshots. The acquisition time is defined as $T_{acq} = KT_s$ where $F_s = 1/T_s$ is the sampling frequency.
- $\mathbf{h} = [h_1\ldots h_N]^T \in \mathbb{C}^{N\times 1}$ is the **non-structured channel model**, which includes both **the channel and the array response**.
- $\mathbf{d}(t, f_d, \tau) = [s_{T,i}(t-(K-1)T_s-\tau_i)e^{j2\pi f_{d,i}(t-(K-1)T_s)}, \ldots, s_{T,i}(t-\tau_i)e^{j2\pi f_{d,i}t}] \in \mathbb{C}^{1\times K}$ is the received GNSS baseband signal for the i-th satellite.
- $\mathbf{N}(t) = [\mathbf{n}(t-(K-1)T_s)\ldots\mathbf{n}(t)] \in \mathbb{C}^{N\times K}$ is a complex, circularly symmetric Gaussian vector process with a zero-mean, temporally white and **spatially colored** with an arbitrary (also unknown) **spatial covariance matrix** $\mathbf{Q} \in \mathbb{C}^{N\times N}$ that **models both the noise and other non desirable terms such as interferences**.

Detection theory

Binary hypothesis testing problem:

$$\mathcal{H}_1 : \mathbf{X}(t) = \mathbf{hd}(t, f_d, \tau) + \mathbf{N}(t) \tag{6}$$

$$\mathcal{H}_0 : \mathbf{X}(t) = \mathbf{N}(t), \tag{7}$$

where $\mathcal{H}_0$ is the *null hypothesis*, when there is no signal present, and $\mathcal{H}_1$ is the *alternative hypothesis*, when the searched signal is present.

Neymann-Pearson (NP) detector

Likelihood Ratio Test (LRT):

$$L(\mathbf{X}) = \frac{p(\mathbf{X};\mathbf{Q},\boldsymbol{\theta}_a,\mathcal{H}_1)}{p(\mathbf{X};\mathbf{Q},\mathcal{H}_0)} = \frac{\frac{1}{\pi^{NK}\det(\mathbf{Q})^K}\exp\left\{-\mathrm{Tr}\{\mathbf{Q}^{-1}\mathbf{C}\}\right\}}{\frac{1}{\pi^{NK}\det(\mathbf{Q})^K}\exp\left\{-\mathrm{Tr}\{\mathbf{Q}^{-1}\hat{\mathbf{R}}_{\mathbf{xx}}\}\right\}} > \gamma, \tag{8}$$

where the PDF of a complex multivariate Gaussian vector for K snapshots is used, and

$$\mathbf{C} = \hat{\mathbf{R}}_{\mathbf{xx}} - \hat{\mathbf{r}}_{\mathbf{xd}}\mathbf{h}^H - \mathbf{h}\hat{\mathbf{r}}_{\mathbf{xd}}^H + \mathbf{h}\hat{R}_{\mathbf{dd}}\mathbf{h}^H, \tag{9}$$

with

- $\hat{\mathbf{R}}_{\mathbf{xx}} = \frac{1}{K}\mathbf{X}\mathbf{X}^H$ is **the autocorrelation matrix estimation**
- $\hat{\mathbf{r}}_{\mathbf{xd}} = \frac{1}{K}\mathbf{X}\mathbf{d}^H$ is **the cross-correlation vector estimation**
- $\hat{R}_{\mathbf{dd}} = \frac{1}{K}\mathbf{d}\mathbf{d}^H$ is **the PRN code autocorrelation estimation**

Generalized Likelihood Ratio Test (GLRT) detector

GLRT criterion: assume no *a priori* knowledge of the PDFs parameters and replace them by their respective Maximum Likelihood Estimators (MLE).

GLRT expression:

$$L(\mathbf{X}) = \frac{p(\mathbf{X};\hat{\mathbf{Q}}_{\mathcal{H}_1},\hat{\boldsymbol{\theta}}_a,\mathcal{H}_1)}{p(\mathbf{X};\hat{\mathbf{Q}}_{\mathcal{H}_0},\mathcal{H}_0)} = \frac{\frac{1}{\pi^{NK}\det(\hat{\mathbf{Q}}_{\mathcal{H}_1})^K}\exp\left\{-\mathrm{Tr}(\hat{\mathbf{Q}}_{\mathcal{H}_1}^{-1}\mathbf{C})\right\}}{\frac{1}{\pi^{NK}\det(\hat{\mathbf{Q}}_{\mathcal{H}_0})^K}\exp\left\{-\mathrm{Tr}(\hat{\mathbf{Q}}_{\mathcal{H}_0}^{-1}\hat{\mathbf{R}}_{\mathbf{xx}})\right\}} > \gamma, \tag{10}$$

where $(\hat{\cdot})$ is the MLE of the signal and noise parameters.

Maximum Likelihood Estimators [FP06]

$$\hat{\mathbf{Q}}_{\mathcal{H}_1} = \mathbf{C}\big|_{\mathbf{h}=\hat{\mathbf{h}},f_d=\hat{f}_d,\tau=\hat{\tau}} \tag{11}$$

$$\hat{\mathbf{Q}}_{\mathcal{H}_0} = \mathbf{C}\big|_{\mathbf{h}=\mathbf{0}} = \hat{\mathbf{R}}_{\mathbf{xx}} \tag{12}$$

$$\hat{\mathbf{h}} = \hat{\mathbf{r}}_{\mathbf{xd}}\hat{R}_{\mathbf{dd}}^{-1}\big|_{\mathbf{Q}_{\mathcal{H}_1}=\hat{\mathbf{Q}}_{\mathcal{H}_1},f_d=\hat{f}_d,\tau=\hat{\tau}} \tag{13}$$

$$\hat{f}_d,\hat{\tau} = \arg\min_{f_d,\tau}\ln(\det(\mathbf{W}(f_d,\tau))), \tag{14}$$

where $\mathbf{W}(f_d,\tau) = \hat{\mathbf{R}}_{\mathbf{xx}} - \hat{\mathbf{r}}_{\mathbf{xd}}(f_d,\tau)\hat{R}_{\mathbf{dd}}^{-1}\hat{\mathbf{r}}_{\mathbf{xd}}(f_d,\tau)^H = \hat{\mathbf{Q}}_{\mathcal{H}_1}\big|_{\mathbf{h}=\hat{\mathbf{h}},f_d,\tau}$.

GLRT statistics

Inserting (11) and (12) in (10), we obtain the test statistic function [Arr12]:

$$\boxed{T_{\mathrm{GL}}(\mathbf{X}) = \max_{f_d,\tau} \left\{ \hat{\mathbf{r}}_{\mathbf{xd}}^H(f_d,\tau)\hat{R}_{\mathbf{dd}}^{-1}\hat{\mathbf{R}}_{\mathbf{xx}}^{-1}\hat{\mathbf{r}}_{\mathbf{xd}}(f_d,\tau) \right\} > \gamma}, \tag{15}$$

Assuming $\hat{\mathbf{R}}_{\mathbf{xx}} \simeq \mathbf{R}_{\mathbf{xx}}$, $T_{\mathrm{GL}}(\mathbf{X})$ is distributed as:

$$T_{\mathrm{GL}}(\mathbf{X}) \sim \begin{cases} \chi^2_{2N}(\delta_{T_{\mathrm{GL}};\mathcal{H}_1}), & \text{in } \mathcal{H}_1, \\ \chi^2_{2N}(\delta_{T_{\mathrm{GL}};\mathcal{H}_0} = 0), & \text{in } \mathcal{H}_0, \end{cases} \tag{16}$$

GLRT theoretical performance

$$P_{fa}(\gamma) = \exp\left\{ \frac{-\gamma}{2\sigma^2_{T_{\mathrm{GL}}}} \right\} \sum_{k=0}^{N-1} \frac{1}{k!} \left(\frac{\gamma}{2\sigma^2_{T_{\mathrm{GL}}}} \right)^k, \tag{17}$$

$$P_d(\gamma) = \mathrm{Q}_N \left(\frac{\sqrt{\delta_{T_{\mathrm{GL}}}(\hat{\mathbf{R}}_{\mathbf{xx}},\mathbf{h})}}{\sigma_{T_{\mathrm{GL}}}}, \frac{\sqrt{\gamma}}{\sigma_{T_{\mathrm{GL}}}} \right), \tag{18}$$

where $\sigma^2_{T_{\mathrm{GL}}} = \frac{1}{2K}$ and Q_N is the generalized Marcum Q-function of order N. **The detector enjoys a Constant False Alarm Rate (CFAR) condition** as $P_{fa}(\gamma)$ does not depend on $\mathbf{X}$.

GLRT performance

The chi-square non-centrality parameter can be expressed as:

$$\delta_{T_{\mathrm{GL}}}(\hat{\mathbf{R}}_{\mathbf{xx}}, \mathbf{h}) = \hat{R}_{\mathbf{dd}} \mathbf{h}^H \hat{\mathbf{R}}_{\mathbf{xx}}^{-1} \mathbf{h} \simeq \mathbf{h}^H \mathbf{R}_{\mathbf{xx}}^{-1} \mathbf{h}. \tag{19}$$

Uniformly Most Powerful (UMP) condition

A UMP detector has the highest possible P_d for a given P_{fa}.
Karlin-Rubin Theorem: Suppose that $T(\mathbf{X})$ is a sufficient statistics for $\boldsymbol{\theta}$, and the family of PDFs associated to $T(\mathbf{X})$ has a Monotone Likelihood Ratio (MLR). Then, the test that rejects $\mathcal{H}_0$ if an only if $T(\mathbf{X}) > \gamma$ is a UMP test.
We check $T_{\mathrm{GL}}(\mathbf{X})$ against the MLR condition as

$$\frac{p(T_{\mathrm{GL}}(\mathbf{X}); \delta_2)}{p(T_{\mathrm{GL}}(\mathbf{X}); \delta_1)} = \frac{p(\chi^2_{2N}(\delta_2))}{p(\chi^2_{2N}(\delta_1))}, \tag{20}$$

where $\delta_1 = \delta_{T_{\mathrm{GL}}}(\hat{\mathbf{R}}_{\mathbf{xx}}, \mathbf{h}_1)$ and $\delta_2 = \delta_{T_{\mathrm{GL}}}(\hat{\mathbf{R}}_{\mathbf{xx}}, \mathbf{h}_2)$ are two possible values for the non-centrality parameter of the chi-square defied in (19). The ratio is monotone non-decreasing for all $\delta_2 > \delta_1$. **The GLRT for GNSS array-based acquisition is a UMP test**.

Simulation results: theoretical PDFs and histograms

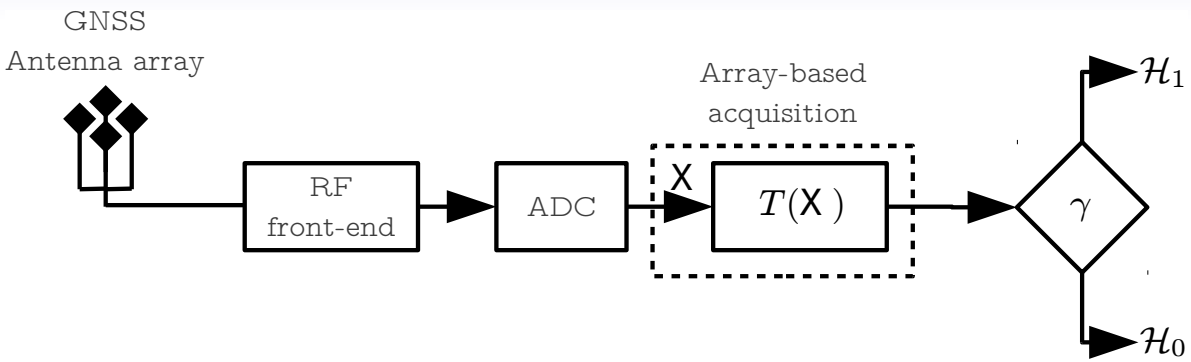

Figure: Array-based GNSS acquisition concept.

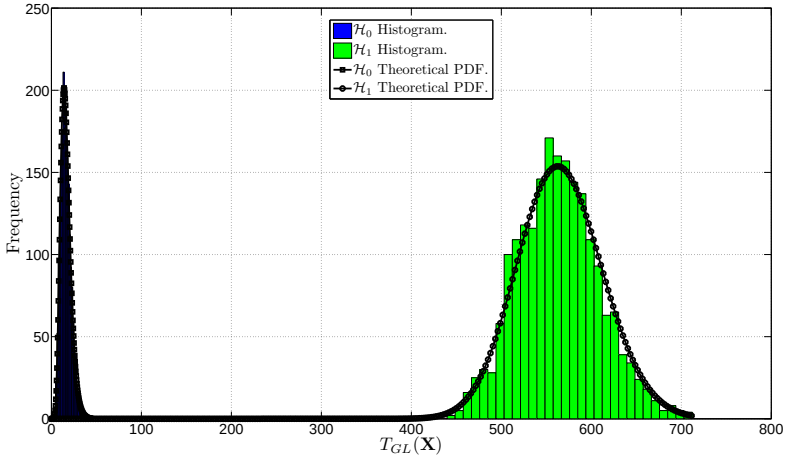

(a) $T_{\mathrm{GL}}(\mathbf{X})$

Figure: Histogram and theoretical PDF in both $\mathcal{H}_1$ and $\mathcal{H}_0$ acquisition hypotheses for Galileo E1 signal acquisition simulation (CN0=38 dB-Hz, no interferences).

GLRT interference rejection capability

Assume M **uncorrelated interferences** impinging into the array through a **channel matrix** $\mathbf{H}_{\mathrm{i}} = [\mathbf{h}_{\mathrm{i},1}, \ldots, \mathbf{h}_{\mathrm{i},M}] \in \mathbb{C}^{N\times M}$ and an **arbitrary basis function matrix** $\mathbf{D}_{\mathrm{i}} = [\mathbf{d}_{\mathrm{i},1}^T, \ldots, \mathbf{d}_{\mathrm{i},M}^T]^T \in \mathbb{C}^{M\times K}$. Then, the noise term is modeled as:

$$\mathbf{N} = \mathbf{H}_{\mathrm{i}}\mathbf{D}_{\mathrm{i}} + \mathbf{N}_w, \tag{21}$$

where $\mathbf{N}_w \sim \mathcal{CN}(\mathbf{0}, \sigma^2\mathbf{I})$. The inverse covariance matrix can be approximated as:

$$\mathbf{Q}^{-1} \simeq \sigma^{-2}\mathbf{P}_{\mathbf{H}_{\mathrm{i}}}^{\perp}, \tag{22}$$

where $\mathbf{P}_{\mathbf{H}_{\mathrm{i}}}^{\perp} = (\mathbf{I} - \mathbf{H}_{\mathrm{i}}(\mathbf{H}_{\mathrm{i}}^H\mathbf{H}_{\mathrm{i}})^{-1}\mathbf{H}_{\mathrm{i}}^H)$ and $\mathbf{R}_{\mathbf{D}_{\mathrm{i}}\mathbf{D}_{\mathrm{i}}} \simeq \mathbf{I}$.
Assuming $\mathrm{E}\{\hat{\mathbf{R}}_{\mathbf{xx}}\} \simeq \mathbf{Q}$, then

$$\boxed{\delta_{T_{\mathrm{GL}}}(\sigma^2, \mathbf{h}, \mathbf{H}_{\mathrm{i}}) = \frac{\mathbf{h}^H\mathbf{P}_{\mathbf{H}_{\mathrm{i}}}^{\perp}\mathbf{h}}{\sigma^2} = \frac{\mathbf{h}^H\mathbf{h}}{\sigma^2} - \frac{\mathbf{h}\mathbf{P}_{\mathbf{H}_{\mathrm{i}}}\mathbf{h}^H}{\sigma^2},} \tag{23}$$

where $\mathbf{P}_{\mathbf{H}_{\mathrm{i}}} = \mathbf{H}_{\mathrm{i}}(\mathbf{H}_{\mathrm{i}}^H\mathbf{H}_{\mathrm{i}})^{-1}\mathbf{H}_{\mathrm{i}}^H$. The SNR can be expressed as $\rho = \frac{\mathbf{h}^H\mathbf{h}}{\sigma^2} = N\frac{P_s}{P_n}$.

GLRT interference rejection capability

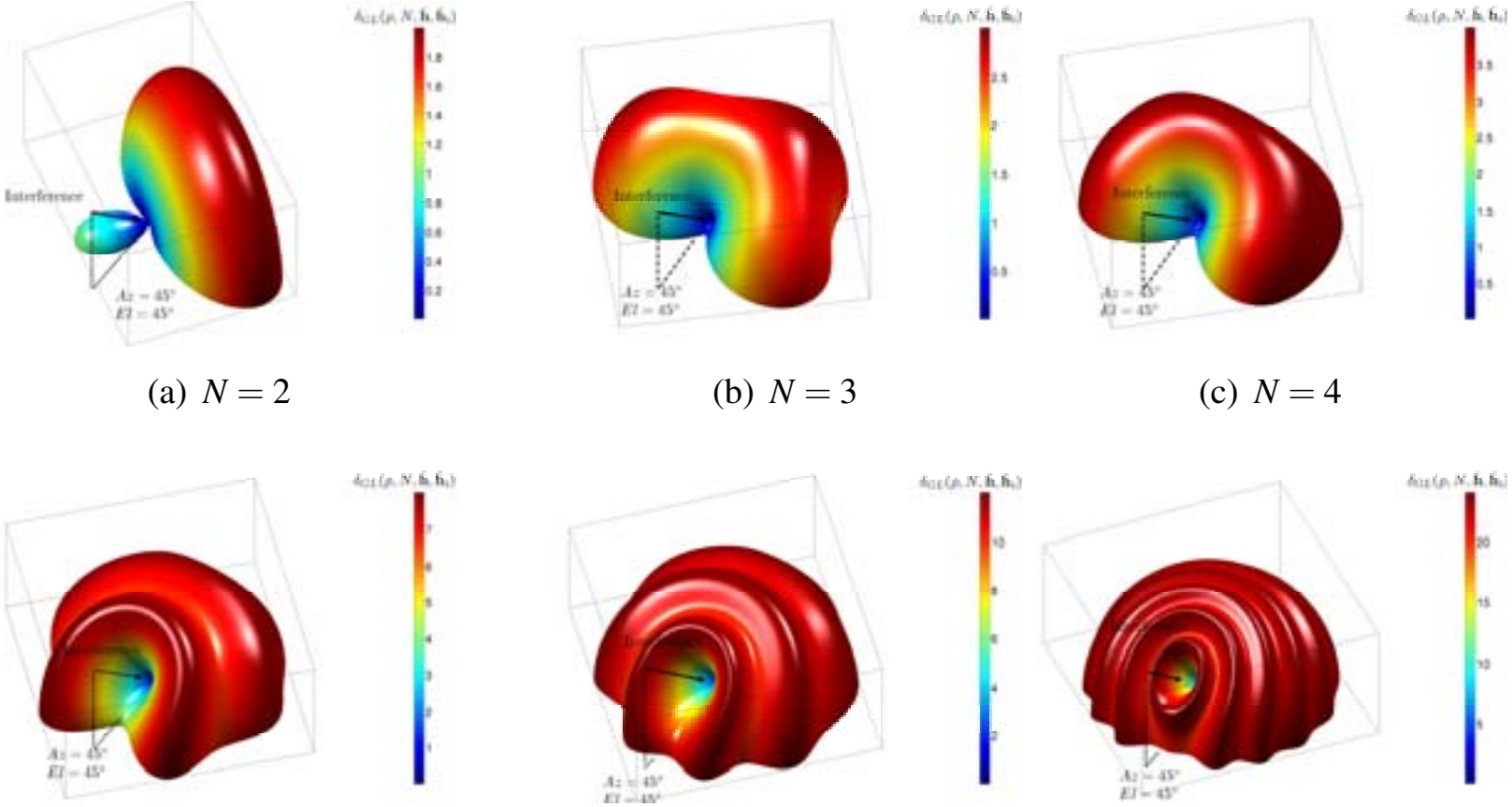

(a) $N = 2$ (b) $N = 3$ (c) $N = 4$

(d) $N = 8$ (e) $N = 12$ (f) $N = 24$

Figure: Evolution of $\delta_{T_{\mathrm{GL}}}(\rho, N, \bar{\mathbf{h}}, \bar{\mathbf{h}}_{\mathrm{i}})$ in the presence of an uncorrelated interference impinging into the array from $Az = 45°$ and $El = 45°$, with $\rho = 1$.

Existing solutions: Acquisition after beamforming

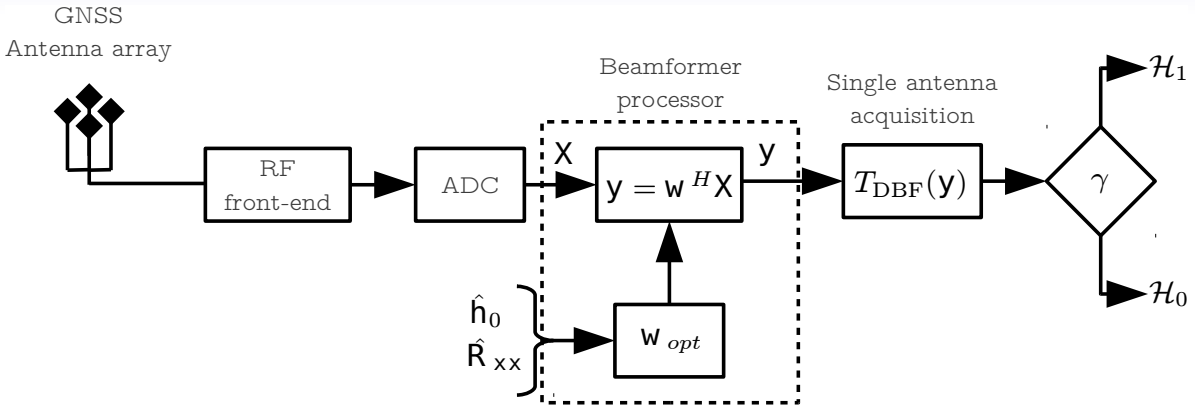

Figure: Acquisition after beamforming concept.

Minimum Variance Distortionless Response (MVDR) GLRT test function

$$T_{\mathrm{MVDR}}(\mathbf{X}) = \frac{\hat{\mathbf{r}}_{\mathbf{xd}}^H(\mathbf{R}_{\mathbf{xx}}^{-1}\mathbf{h}_0)(\mathbf{R}_{\mathbf{xx}}^{-1}\mathbf{h}_0)^H\hat{\mathbf{r}}_{\mathbf{xd}}}{\mathbf{h}_0^H\mathbf{R}_{\mathbf{xx}}^{-1}\mathbf{h}_0} \simeq \frac{1}{\sigma^2}\frac{|\hat{\mathbf{r}}_{\mathbf{xd}}^H\mathbf{P}_{\mathbf{H}_i}^{\perp}\mathbf{h}_0|^2}{\|\mathbf{h}_0^H\mathbf{P}_{\mathbf{H}_i}^{\perp}\|^2}, \tag{24}$$

where $\mathbf{h}_0 \in \mathbb{C}^{N\times 1}$ is the signal **DOA steering vector**.

Power Minimization Beamformer: **signal DOA unavailable**

Minimize the output power establishing a reference antenna

$$\mathbf{h}_0 = [1\,0\ldots 0]. \tag{25}$$

Simulation results: performance in ideal conditions

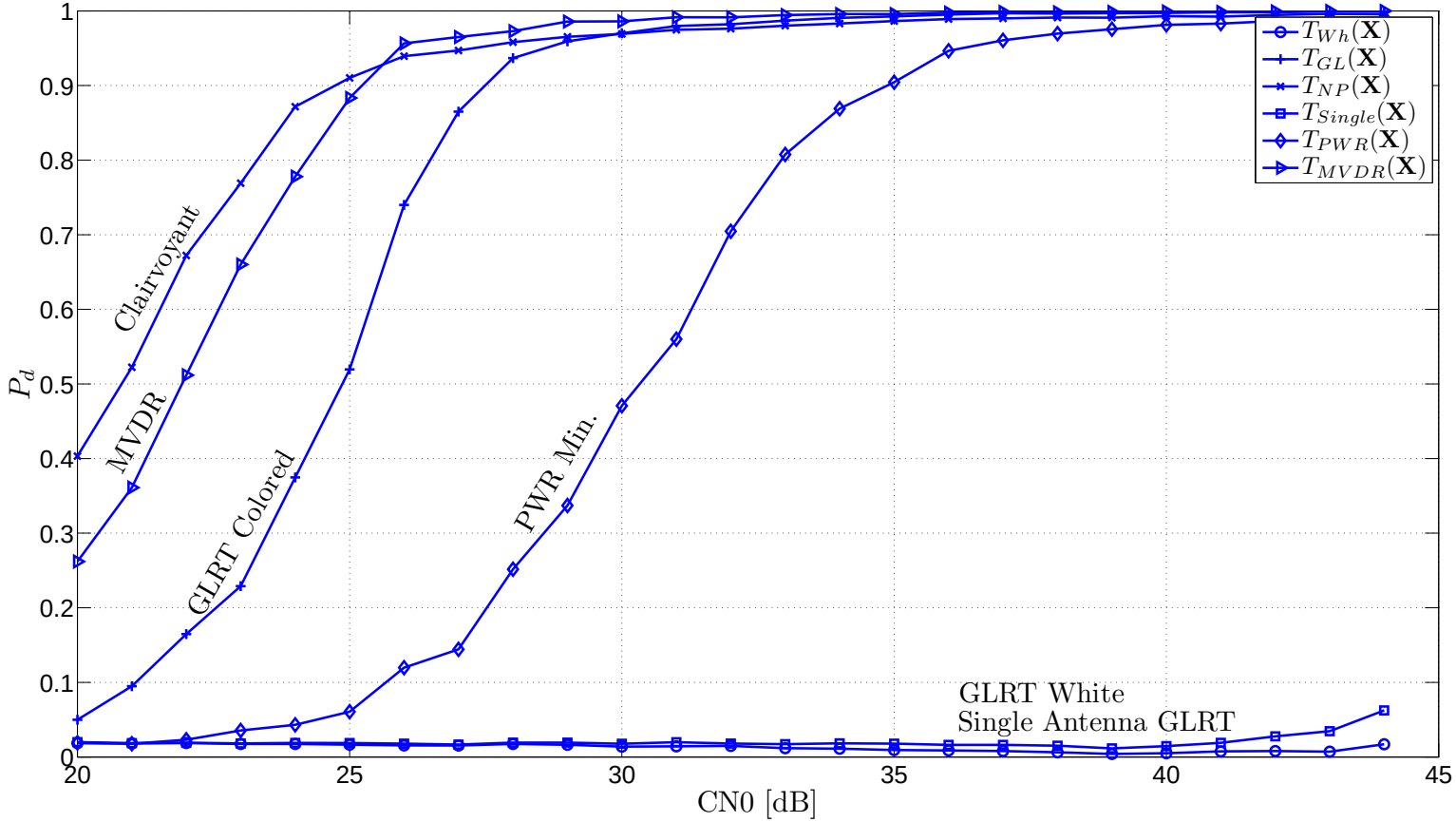

Figure: Galileo E1 acquisition P_d vs. satellite CN0 in the presence of an in-band wideband interference for different algorithms ($IN0 = 85$ **dB-Hz**, $P_{fa} = 0.001, f_s = 6$ MSPS, $T_{acq} = 4$ ms). No pointing error in $T_{\mathrm{MVDR}}(\mathbf{X})$.

Simulation results: performance with pointing error

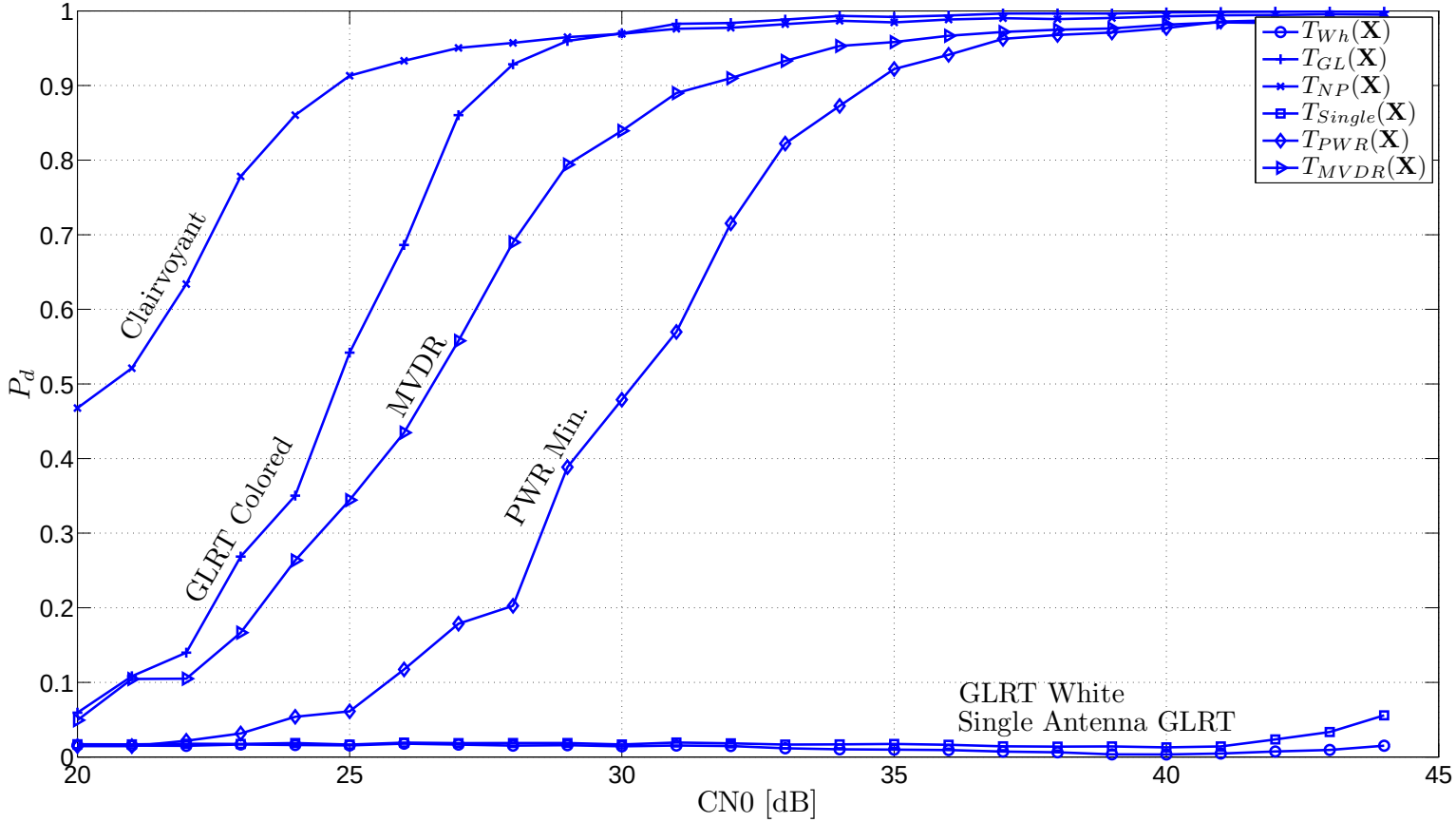

Figure: Galileo E1 acquisition P_d vs. satellite CN0 in the presence of an in-band wideband interference for different algorithms ($IN0 = 85$ **dB-Hz**, $P_{fa} = 0.001$, $f_s = 6$ MSPS, $T_{acq} = 4$ ms). 20° DOA pointing error in $T_{\mathrm{MVDR}}(\mathbf{X})$. (array uncalibrated in acquisition)

Realistic conditions

- **finite sample size**
- **signal quantization effects**
- **satellite signal synchronization errors**

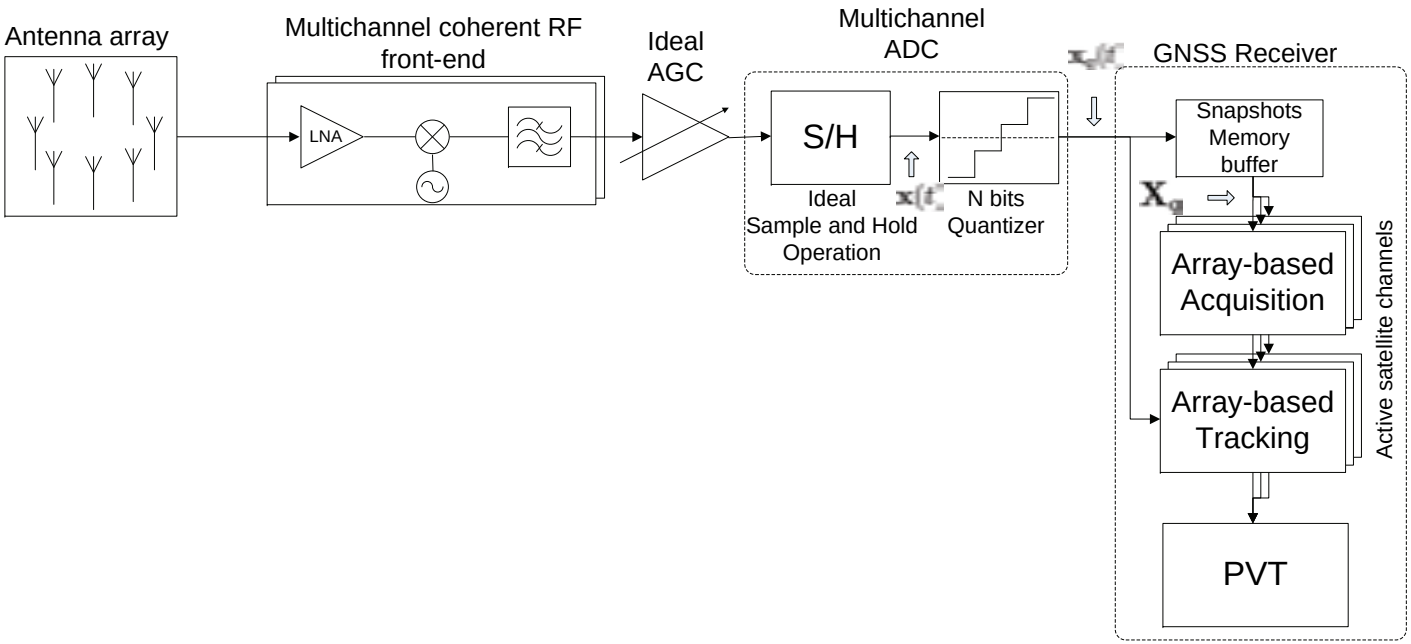

Figure: GNSS receiver block diagram, as simulated.

A Metric to measure the presence of errors in $\hat{\mathbf{R}}_{\mathbf{xx}}$

Geodesic distance: *For any two points inside* $\mathcal{S} = \{\mathbf{R} \in \mathbb{C}^{N\times N} : \mathbf{R}^H = \mathbf{R}, \mathbf{R} \succ \mathbf{0}\}$, *the geodesic distance is the length of the geodesic curve that connects them*:

$$\mathrm{dist}_g(\mathbf{R}_1, \mathbf{R}_2) = \|\mathbf{M}\|_F, \tag{26}$$

where $\|\mathbf{M}\|_F = \sqrt{(\sum_i |\ln(\lambda_i)|^2)}$ stands for the logarithmic version of the Frobenius norm, $\mathbf{M} = \ln(\mathbf{R}_1^{\frac{-1}{2}} \mathbf{R}_2 \mathbf{R}_1^{\frac{-1}{2}})$, and λ_i represents the *i-th* eigenvalue of matrix $\mathbf{R}_1^{\frac{-1}{2}} \mathbf{R}_2 \mathbf{R}_1^{\frac{-1}{2}}$. **The geodesic distance is able to detect differences both in the eigenvectors and in the eigenvalues** of $\mathbf{R}_{\mathbf{xx}}$ and $\hat{\mathbf{R}}_{\mathbf{xx}}$.

Quantization effects in $\hat{\mathbf{R}}_{\mathbf{xx}}$

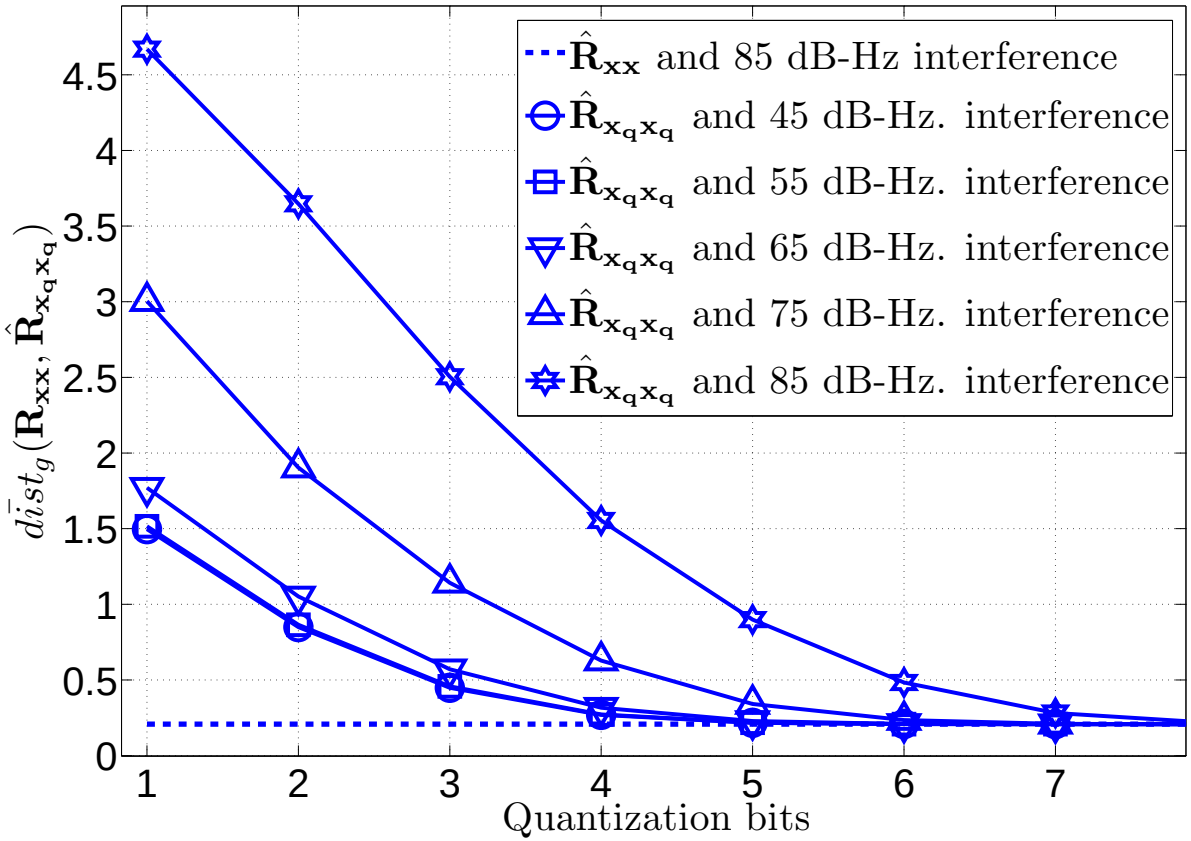

Figure: $\text{dist}_g(\mathbf{R}_{\mathbf{xx}}, \hat{\mathbf{R}}_{\mathbf{x}_q\mathbf{x}_q})$ vs. different quantization bits and **an in-band CW interference impinging into the array** with different $IN0$.

Quantization effects in $\hat{\mathbf{R}}_{\mathbf{xx}}$

Receiver Operating Characteristic (ROC) curve

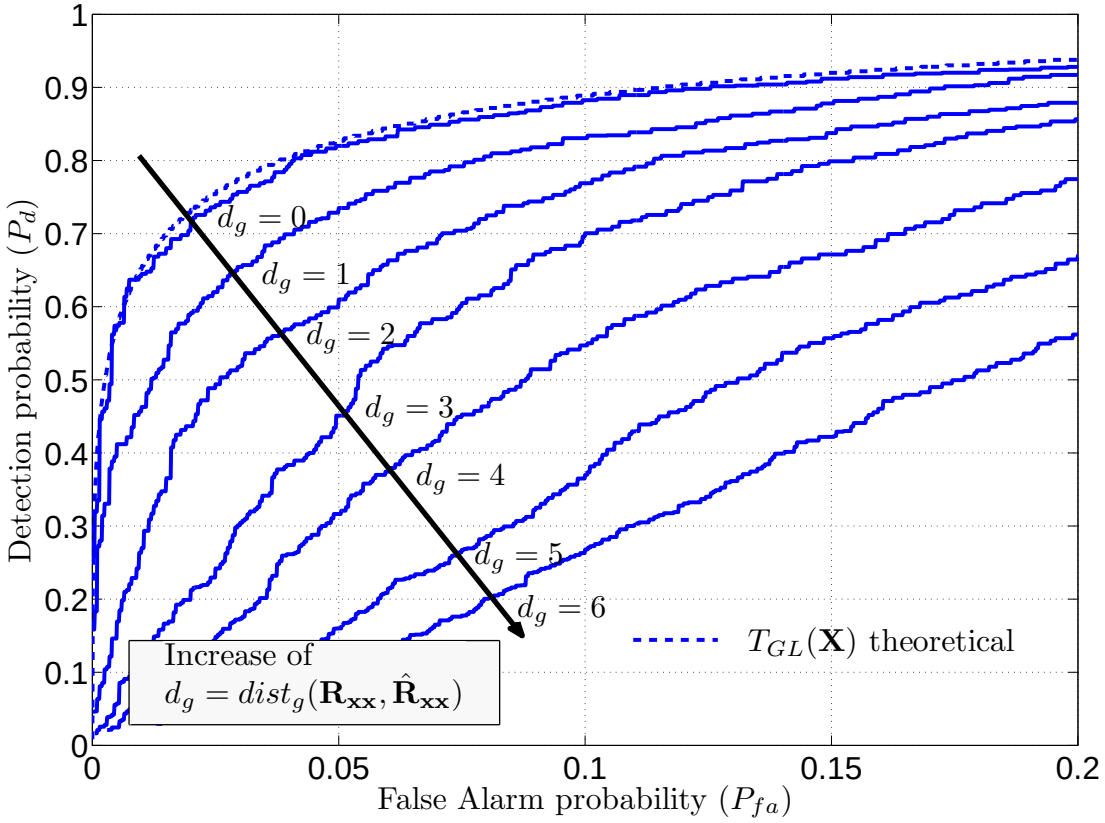

Figure: Effect of the $\text{dist}_g(\mathbf{R}_{\mathbf{xx}}, \hat{\mathbf{R}}_{\mathbf{xx}})$ in the acquisition performance of $T_{\text{GL}}(\mathbf{X})$, with **an in-band CWI impinging into the array with** $IN0 = 85$ **dB-Hz**.

Acquisition performance vs. ADC resolution

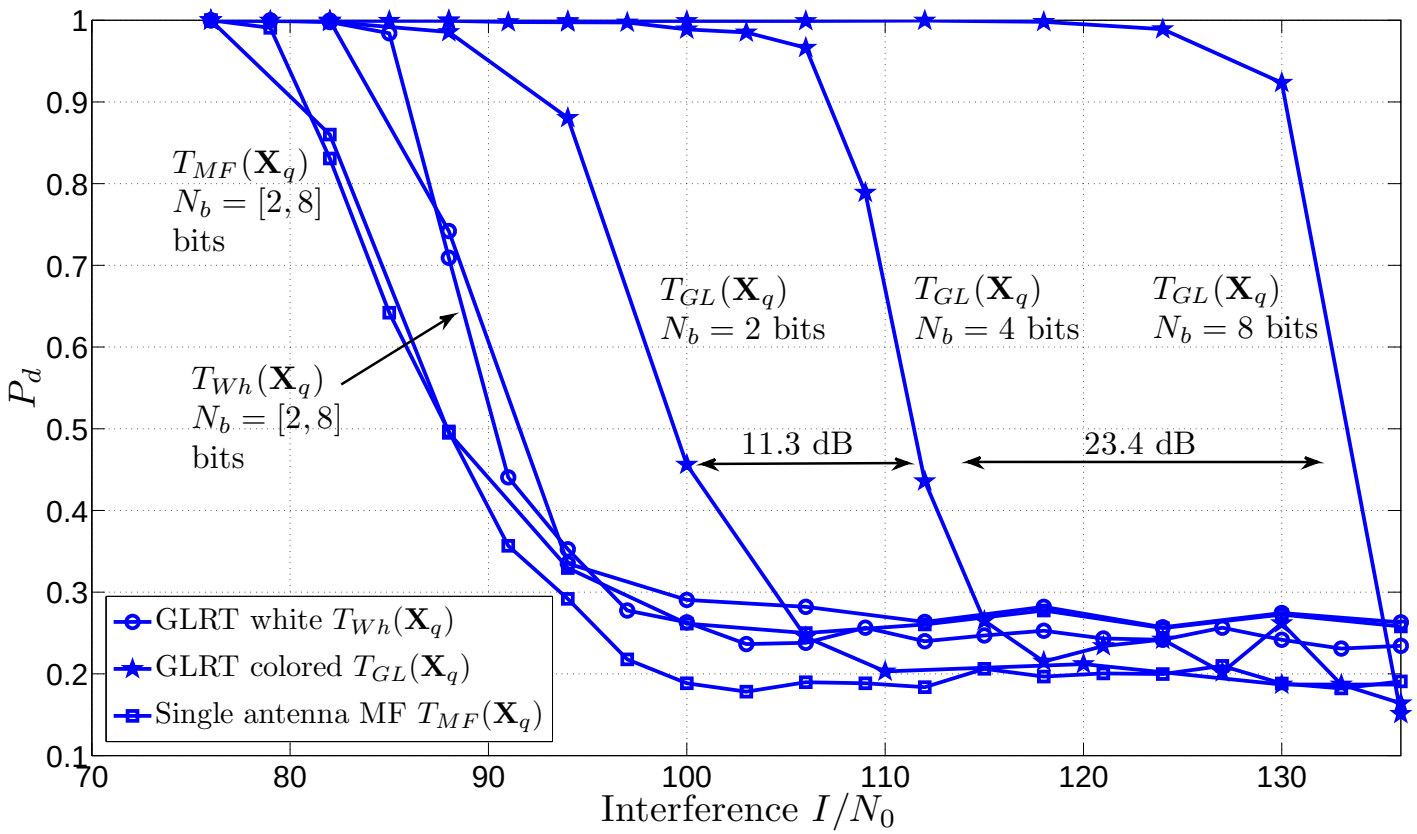

Figure: P_d in an scenario with satellite $CN0 = 44$ dB-Hz, and **an in-band CW interference impinging into the array** with $IN0 = 70 - 136$ dB-Hz, for $P_{fa} = 0.001$ and $N_b = 2 - 8$ bits.

Front-end bandwidth effect in acquisition I

The pre-correlation SNR is defined as $\rho_{acq} = \frac{P'_s}{P'_n}$, where

$$P'_s = P_s \int_{\frac{-1}{2}}^{\frac{1}{2}} G_s(f)|H_{FE}(f)|^2 df, \tag{27}$$

$$P'_n = \frac{N_0}{2} B_{FE} \int_{-\frac{1}{2}}^{\frac{1}{2}} |H_{FE}(f)|^2 df, \tag{28}$$

with

- N_0 is the antenna noise density and B_{FE} is the front-end pass-band bandwidth
- $G_s(f) = \frac{10}{11} G_{BOC(1,1)} + \frac{1}{11} G_{BOC(6,1)}$ is the PSD (for Galileo MBOC(6,1,1/11))
- $H_{FE}(f)$ is the DTFT of the front-end baseband-equivalent impulse response

Considering now $\mathbf{d}' = \mathbf{d} * \mathbf{h}_{FE}$, using Wiener-Khinchine, we compute $R_{\mathbf{d}'\mathbf{d}}$ as:

$$R_{\mathbf{d}'\mathbf{d}}[\tau] = \int_{\frac{-1}{2}}^{\frac{1}{2}} G_s(f) H_{FE}(f) e^{j2\pi f \tau} df, \tag{29}$$

and therefore $P_s R_{\mathbf{d}'\mathbf{d}}[0] = P_s \int_{-0.5}^{0.5} G_s(f) H_{FE}(f) df$. Now considering $H_{FE}(f)$ response of an ideal band-pass filter, then

$$P_s R_{\mathbf{d}'\mathbf{d}}[0] = P_s \int_{-\frac{B_{FE}}{2f_s}}^{\frac{B_{FE}}{2f_s}} G_s(f) = P'_s. \tag{30}$$

Front-end bandwidth effect in acquisition II

Finally, by inserting P'_s and P'_n in the non-centrality parameter of the performance expressions we can write

$$\delta_{T_{\mathrm{GL}}} = \frac{|\mu_{R_{\mathbf{xd}}}|^2}{R_{\mathbf{xx}}} \simeq \frac{P'_s}{P'_n} = \rho_{acq}, \tag{31}$$

which implies that the maximization of ρ_{acq} maximizes the acquisition performance.

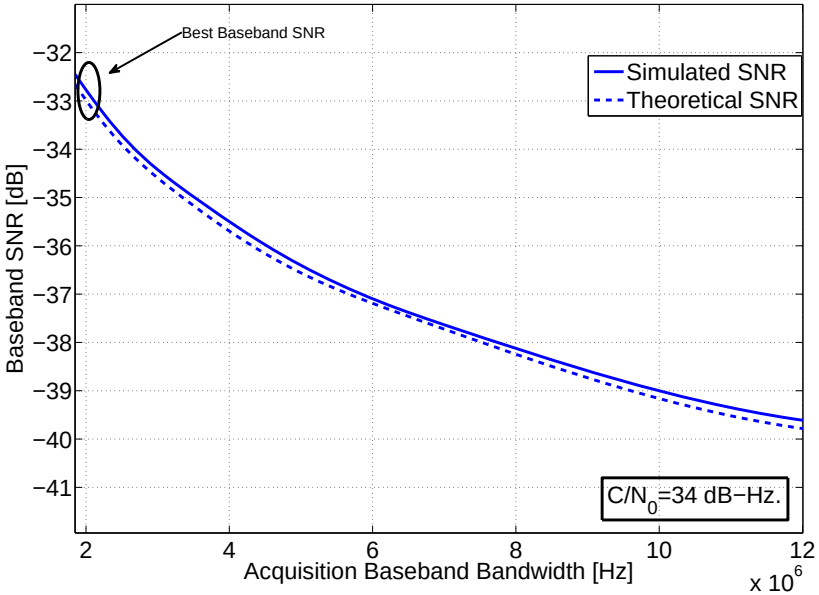

(a) SNR vs. BW

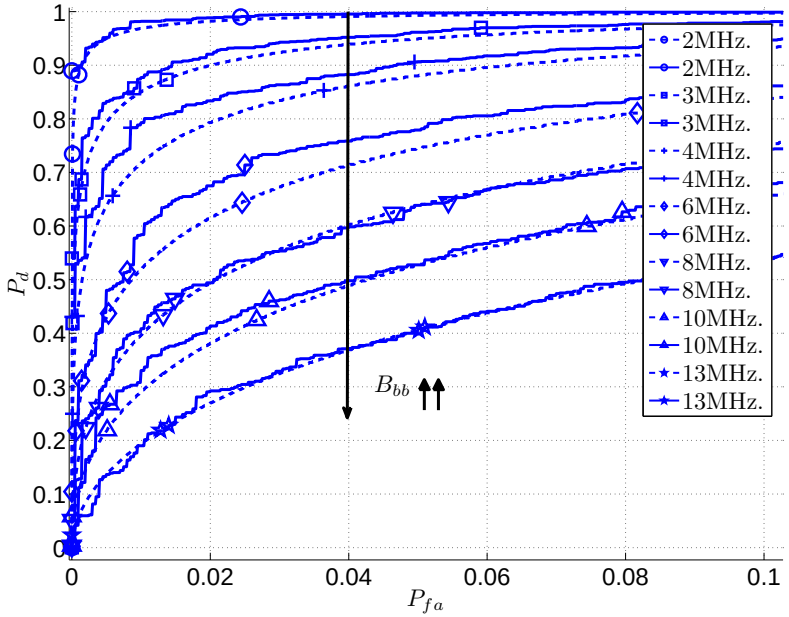

(b) ROC vs. BW

Figure: Theoretical and simulated Galileo E1 MBOC(6,1,1/11) SNR and ROC curves vs. the baseband BW.

Front-end bandwidth effect in acquisition III

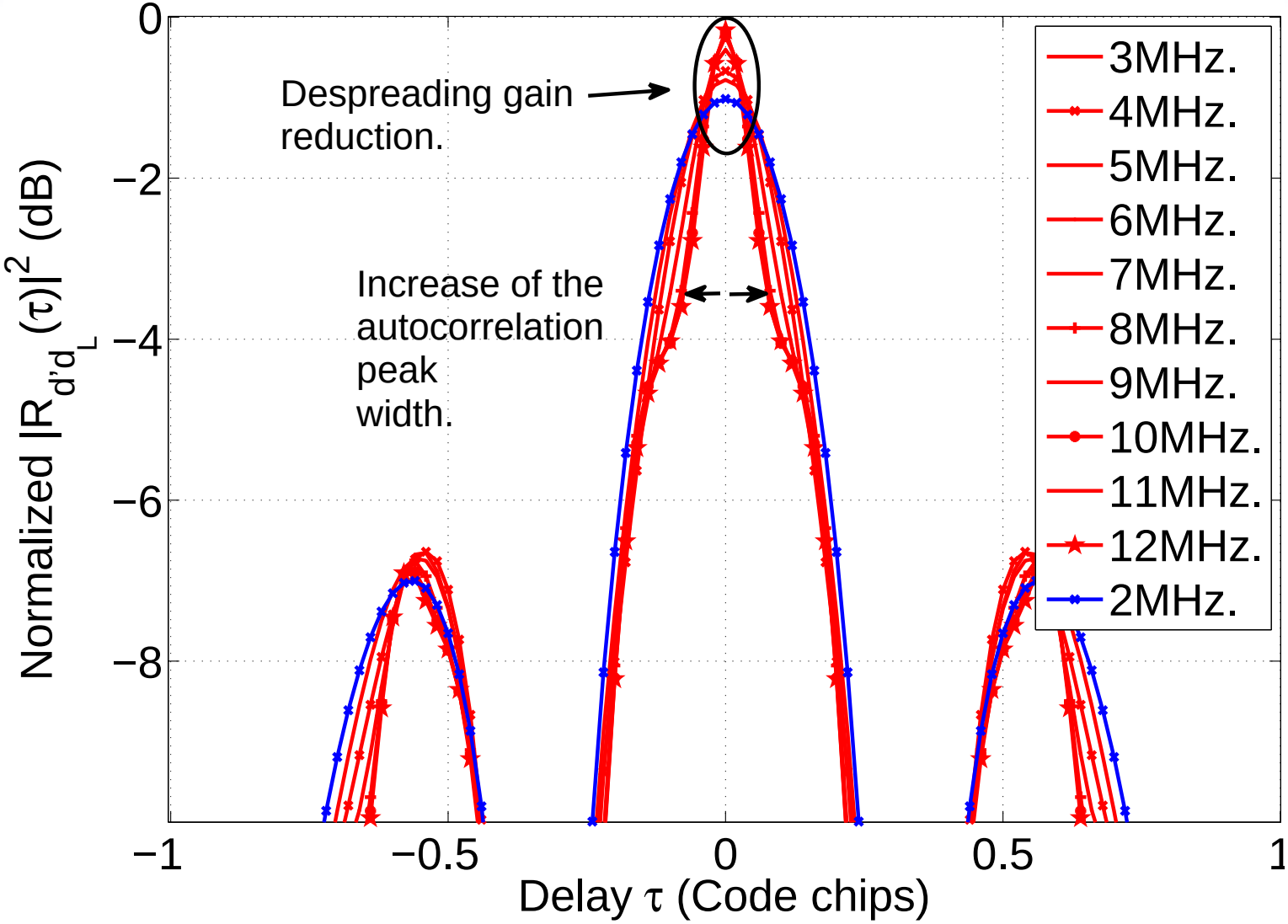

Figure: Autocorrelation of Galileo E1 MBOC(6,1,1/11) signal with the local replica versus τ for different baseband bandwidths.

Objectives

Exploit the spatial diversity in acquisition

- Improve the existing GNSS acquisition algorithms performance.
- **Improve the GNSS interference robustness** proposing **novel array-based acquisition algorithms** using the **statistical detection theory** framework.

Demonstrate the implementation feasibility

- Design and implementation of an array-based GNSS receiver platform
- **Proof-of-concept** of array-based acquisition algorithms working in **real-time**
  - **Interference mitigation**.
  - Performance measurements in **realistic scenarios**.
- Tightly coupled with GNSS software receivers.

Generic GNSS array-based receiver platform

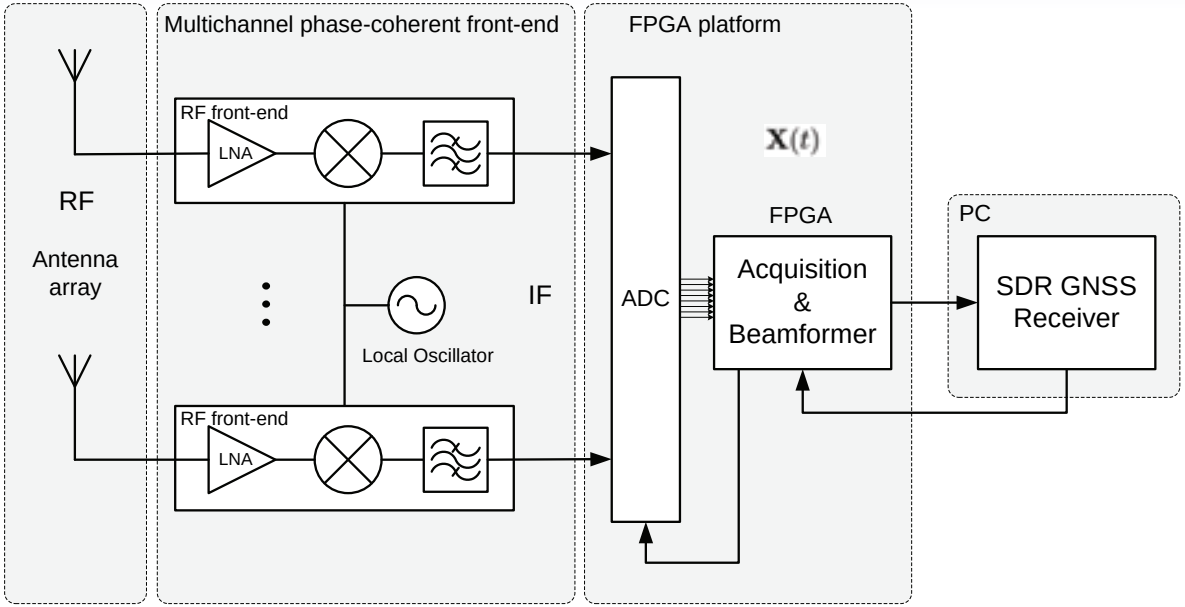

Figure: Simplified system block diagram.

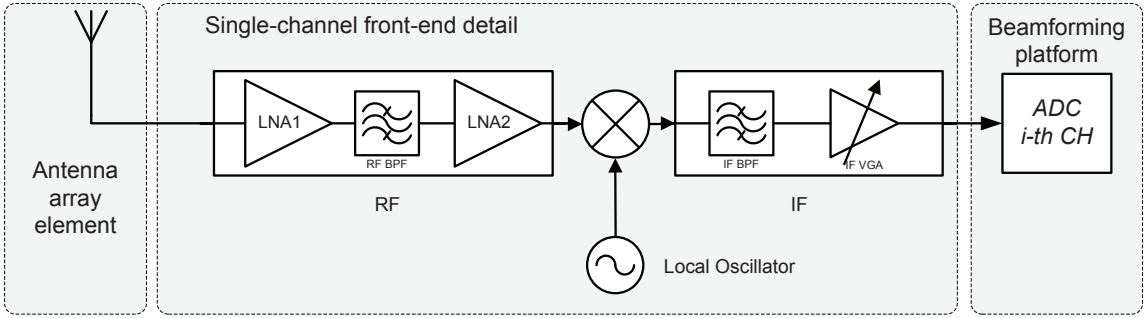

Figure: Simplified front-end for each antenna element.

Front-end requirements overview

Parameter	Effect in Acquisition	Effect in Tracking
↑ Bandwidth (BW)	↓ sensitivity if BW exceeds the main lobe (SNR loss)	↑ $\hat{\tau}$ precision (see RMSE CRB)
↑ Noise Figure (NF)	↓ sensitivity (↓ CN0)	↓ $\hat{\tau}$ precision (↓ CN0)
↑ ADC active bits (N_b)	↑ sensitivity (No CN0 ↓ if $N_b \geq 4$)	↑ sensitivity (No CN0 ↓ if $N_b \geq 4$)
↑ Linearity	↑ interference robustness	↑ interference robustness

Receiver performance bounds

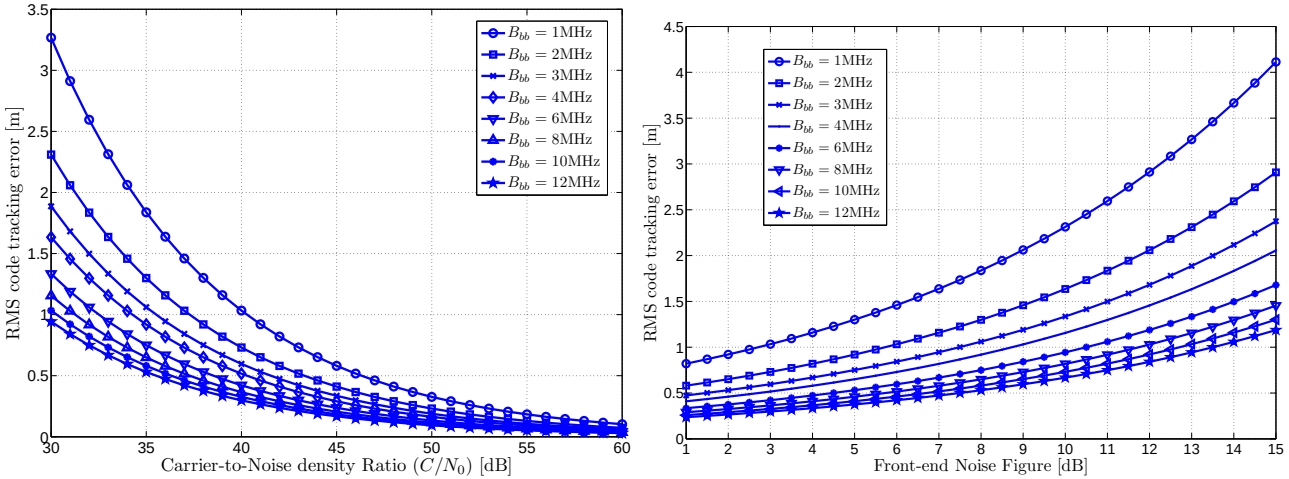

Figure: GPS L1 C/A code tracking Cramér-Rao Bound (CRB) minimum RMSE vs. front-end NF, BW, and signal CN0 [Wei94].

ADC resolution	**CN0 degradation** $f_s \geq 2B_s$	**CN0 degradation** $f_s = 2B_p$
1 bit	1.96 dB	3.5 dB
2 bits	0.55 dB	1.2 dB
3 bits	0.16 dB	0.6 dB
4 bits or more	≤ 0.16	≤ 0.6 dB

Table: GPS L1 C/A CN0 degradation vs. ADC resolution assuming Gaussian noise [Par96].

Front-end specifications

- **Bandwidth, f_s, and Noise Figure (NF)**: set by the desired GNSS performance.
- **Gain**: the thermal noise excites the ADC, thus:

$$G_{\mathrm{FE}} \geq P_{\mathrm{ADC}} - P_n,$$
$$G_{\mathrm{FE}} \geq 10\log\left(\frac{\left(\frac{(V_{\mathrm{LSB}}2^{N_{\mathrm{bits}}-1})^2}{Z_{\mathrm{ADC}}}\right)}{kT_aB_p}\right), \tag{32}$$

where V_{LSB} is the Least Significant Bit voltage (RMS), N_{bits} is the **number of active bits** and $P_n = kT_aB_p$ is the noise power where $k = 1.3806 \times 10^{-23}$ J/K and T_a is the antenna sky temperature, and B_p is the passband bandwidth.

- **Linearity Parameters**: Compression Point (CP) and Third Order Interception Point (IP3) are **set by the maximum admissible input power**

$$P_{\mathrm{int\ max}} = P_{\mathrm{FSR}} - G_{\mathrm{FE}}. \tag{33}$$

where P_{FSR} is the ADC full-scale input power. The front-end should behave linear for an input signal power $P_{in} \leq P_{\mathrm{int\ max}}$.

ADC Particular case: $V_{\mathrm{FSR}} = 2$ Vpp, $Z_{\mathrm{ADC}} = 50\ \Omega$, $P_{\mathrm{FSR}} = 19.1$ dBm, and $N_b = 12$.
FE Specifications: $N_b \geq 4$, $P_{\mathrm{ADC}} \geq -35$ dBm, $P_n = -107.8$ dBm, $G_{\mathrm{FE}} \geq 72.8$ dB
$P_{\mathrm{int\ max}} = P_{\mathrm{FSR}} - G_{\mathrm{FE}} = -53.7$ dBm, $P_{\mathrm{CP}} \geq P_{\mathrm{int\ max}}$ and $P_{\mathrm{IP3}} \geq (P_{\mathrm{int\ max}} + 9.6)$.

Proposed front-end channel architecture and specifications

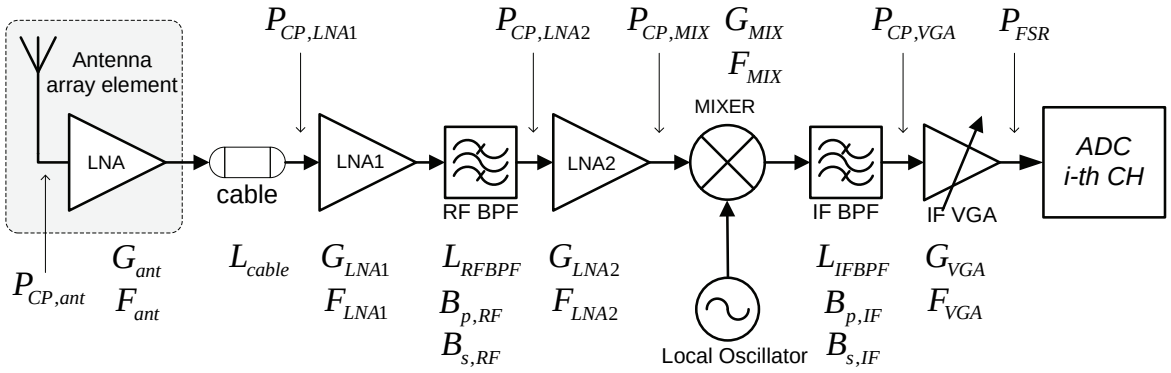

By applying the Friis formula we obtain the overall NF as:

$$F_{FE} = F_{\text{ant}} + \frac{L_{\text{cable}} - 1}{G_{\text{ant}}} + \frac{F_{\text{LNA1}} - 1}{\frac{G_{\text{ant}}}{L_{\text{cable}}}} + \frac{L_{\text{RF\_BPF}} - 1}{\frac{G_{\text{ant}} G_{\text{LNA1}}}{L_{\text{cable}}}} + \frac{F_{\text{LNA2}} - 1}{\frac{G_{\text{ant}} G_{\text{LNA1}}}{L_{\text{cable}} L_{\text{RF\_BPF}}}} + \\ + \frac{F_{\text{MIX}} - 1}{\frac{G_{\text{ant}} G_{\text{LNA1}} G_{\text{LNA2}}}{L_{\text{cable}} L_{\text{RF\_BPF}}}} + \frac{L_{\text{IF\_BPF}} - 1}{\frac{G_{\text{ant}} G_{\text{LNA1}} G_{\text{LNA2}} G_{\text{MIX}}}{L_{\text{cable}} L_{\text{RF\_BPF}}}} + \frac{F_{\text{VGA}} - 1}{\frac{G_{\text{ant}} G_{\text{LNA1}} G_{\text{LNA2}} G_{\text{MIX}}}{L_{\text{cable}} L_{\text{RF\_BPF}} L_{\text{IF\_BPF}}}}, \tag{34}$$

and

Component	Compression point	Computed min. value
Antenna LNA	$P_{CP,\text{ant}} \geq P_{CP,\text{LNA1}} - G_{\text{ant}} + L_{\text{cable}}$	-55.9 dBm
LNA1	$P_{CP,\text{LNA1}} \geq P_{CP,\text{LNA2}} - G_{\text{LNA1}} + L_{\text{RF\_BPF}}$	-44.9 dBm
LNA2	$P_{CP,\text{LNA2}} \geq P_{CP,\text{MIX}} - G_{\text{LNA2}}$	-25.9 dBm
Mixer	$P_{CP,\text{MIX}} \geq P_{CP,\text{VGA}} - G_{\text{MIX}} + L_{\text{IF\_BPF}}$	-10.9 dBm
VGA	$P_{CP,\text{VGA}} \geq P_{\text{FSR}} - G_{\text{VGA}}$	-15.9 dBm

Antenna array elements

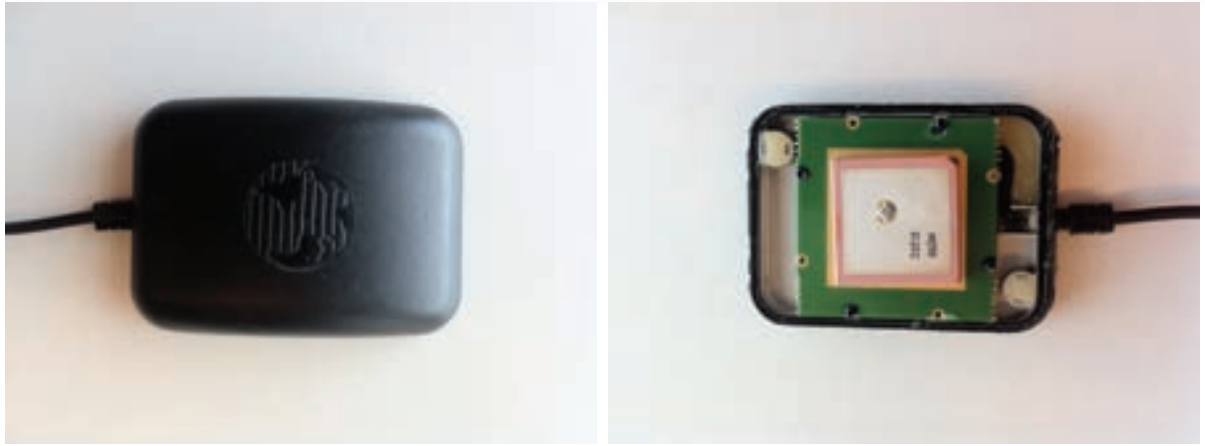

Figure: Garmin GA27c active antenna.

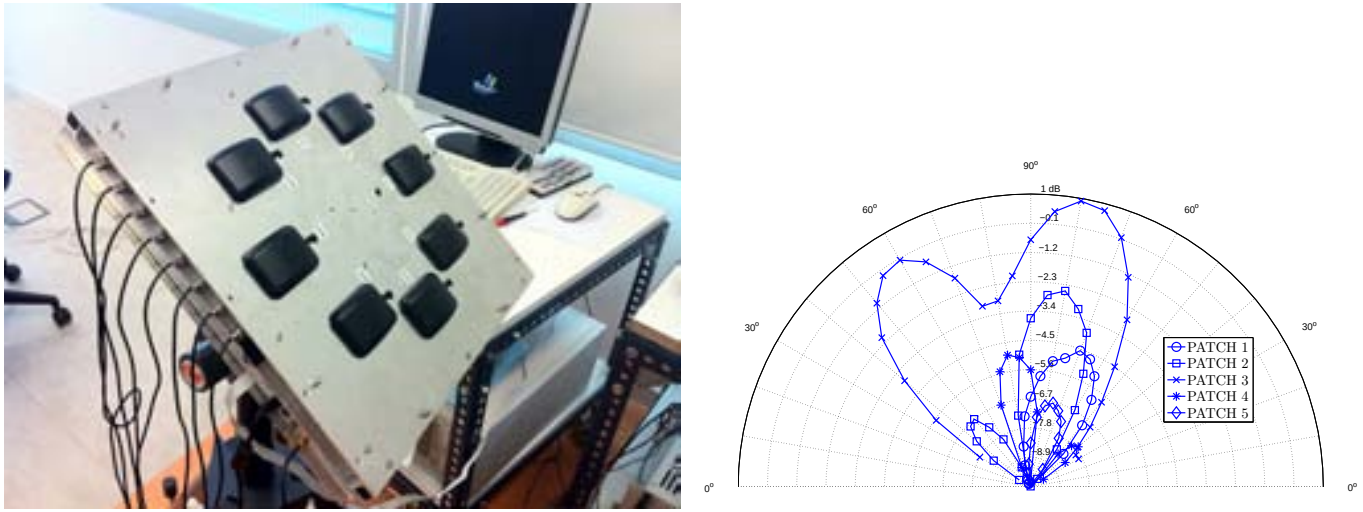

Figure: Antenna array prototype and differences between radiation patterns of some antenna elements in elevation.

Local Oscillator distribution network

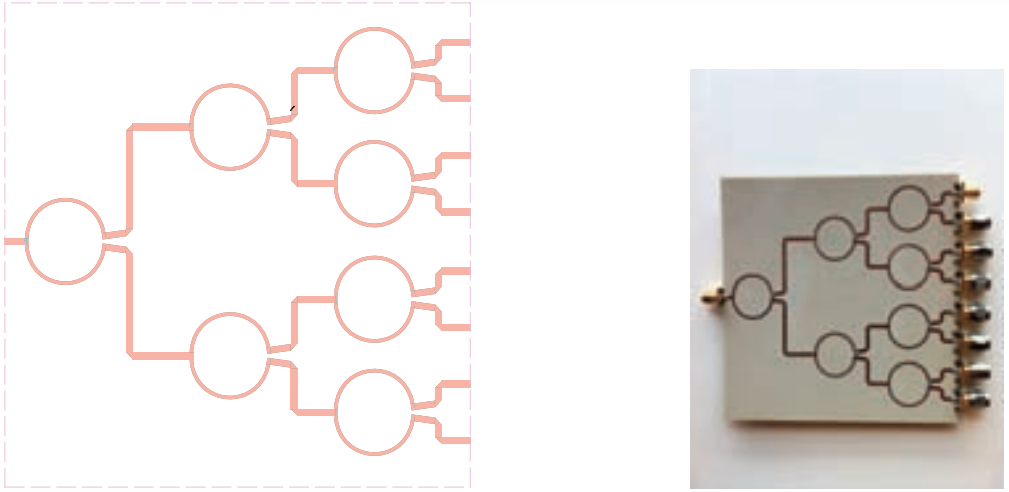

Figure: Eight ports Wilkinson PCB layout and prototype.

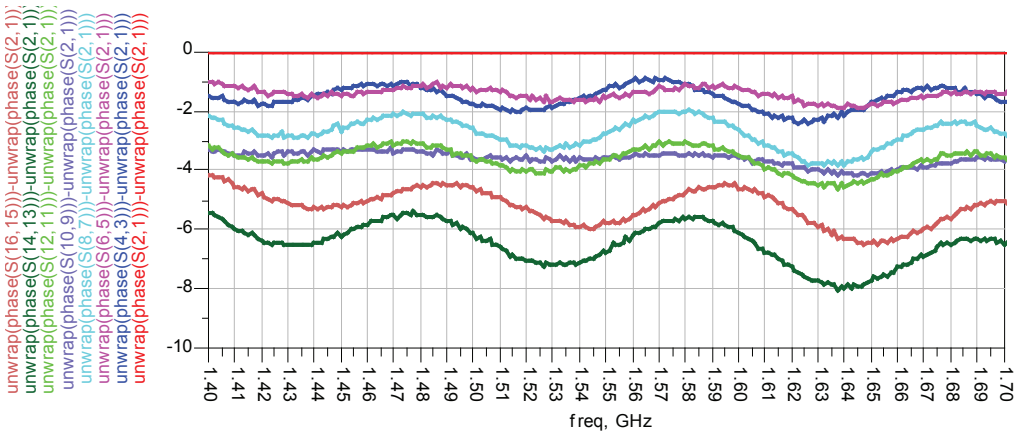

Figure: Measured output signal phase differences [°].

Multichannel PCB implementation

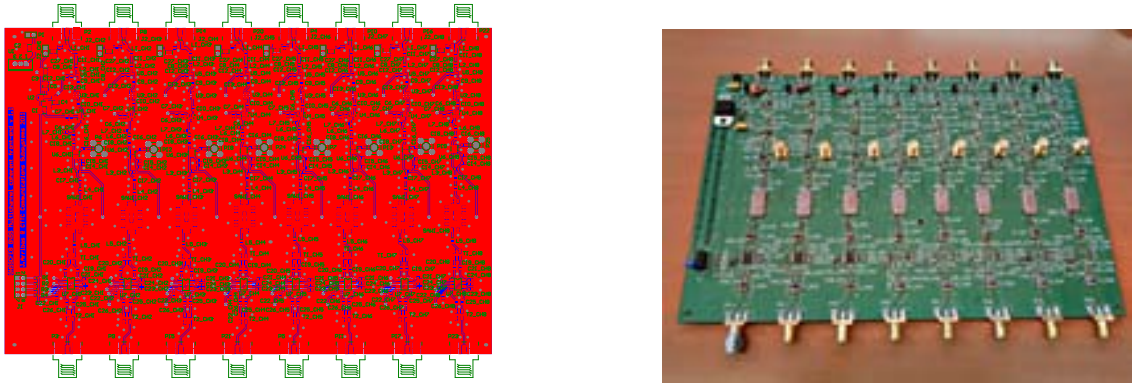

Figure: PCB design and prototype.

Figure: Front-end housing and setup on the antenna-array frame.

Front-end channel design specifications and prototype performance summary

Parameter	Simulated Value	Measured Value	Specification
RF frequency	1575.42 MHz	1575.42 MHz	1575.42 MHz
IF frequency	70 MHz	69.9988 MHz	70 MHz (*)
Passband bandwidth (B_p)	17.8 MHz	17.5 MHz	$\geq$ 12 MHz
Stopband bandwidth (B_s)	20 MHz	22 MHz	$\leq$ 20 MHz (*)
G_{FE}	73.9 dB	$58 + G_{ant} = 73$ dB	$\geq$ 72.8 dB
NF_{FE}	2.178 dB	2.18 dB	$\leq$ 4 dB
$P_{CP,\mathrm{FE}}$	—	-65.3 dBm	> -44.9 dBm (*)
$P_{IP3,\mathrm{FE}}$	—	$-65.3 + 9.6 = -54.7$ dBm	> -35.3 dBm (*)
Image rejection	60.2 dB	57 dB	$\geq$ 40 dB
Phase noise (10 kHz)	-75.65 dBc	-82 dBc	—

Table: Simulated and measured front-end performance compared to design specifications.

- **Out-of-specs linearity**: considering an in-band interference signal present at the antenna terminals with $P_{int} = P_{CP,\mathrm{FE}}$, **the front-end linearity is sufficient to test the algorithms interference mitigation capability for** $IN0 \leq 113$ **dB-Hz** considering $T_a = 100$ K.

FPGA Digital processing detailed block diagram

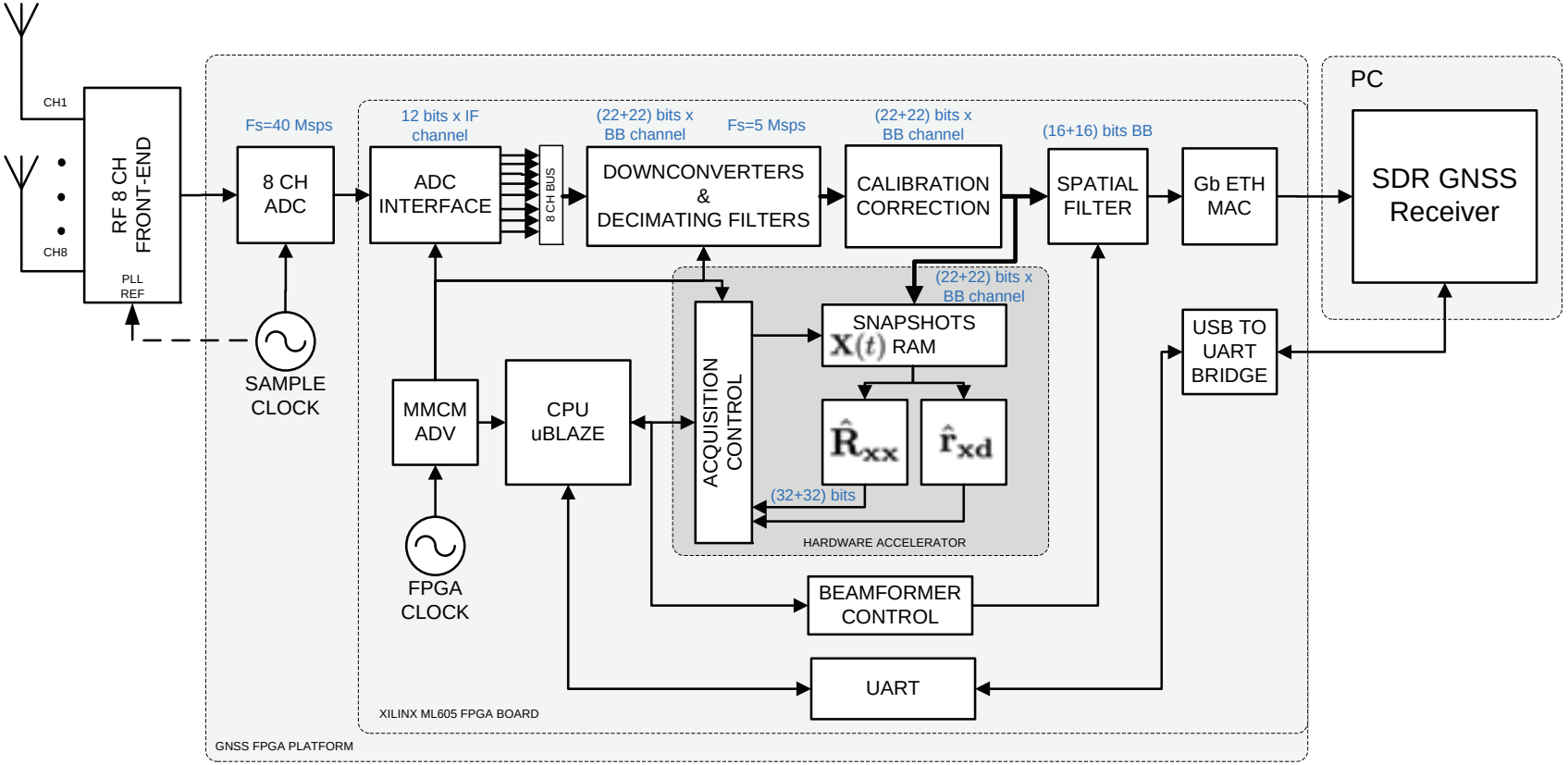

Autocorrelation matrix estimation implementation

$$\hat{\mathbf{R}}_{\mathbf{xx}} = \frac{1}{K}\mathbf{X}\mathbf{X}^H =$$

$$= \frac{1}{K}\left[\sum_{k=1}^{K}\mathbf{x}(k)x_1^*(k), \quad \ldots, \quad \sum_{k=1}^{K}\mathbf{x}(k)x_N^*(k)\right] =$$

$$= \frac{1}{K}\begin{bmatrix} \sum_{k=1}^{K} x_1(k)x_1^*(k) & \ldots & \sum_{k=1}^{K} x_1(k)x_N^*(k) \\ \vdots & \ddots & \vdots \\ \sum_{k=1}^{K} x_N(k)x_1^*(k) & \ldots & \sum_{k=1}^{K} x_N(k)x_N^*(k) \end{bmatrix}. \tag{35}$$

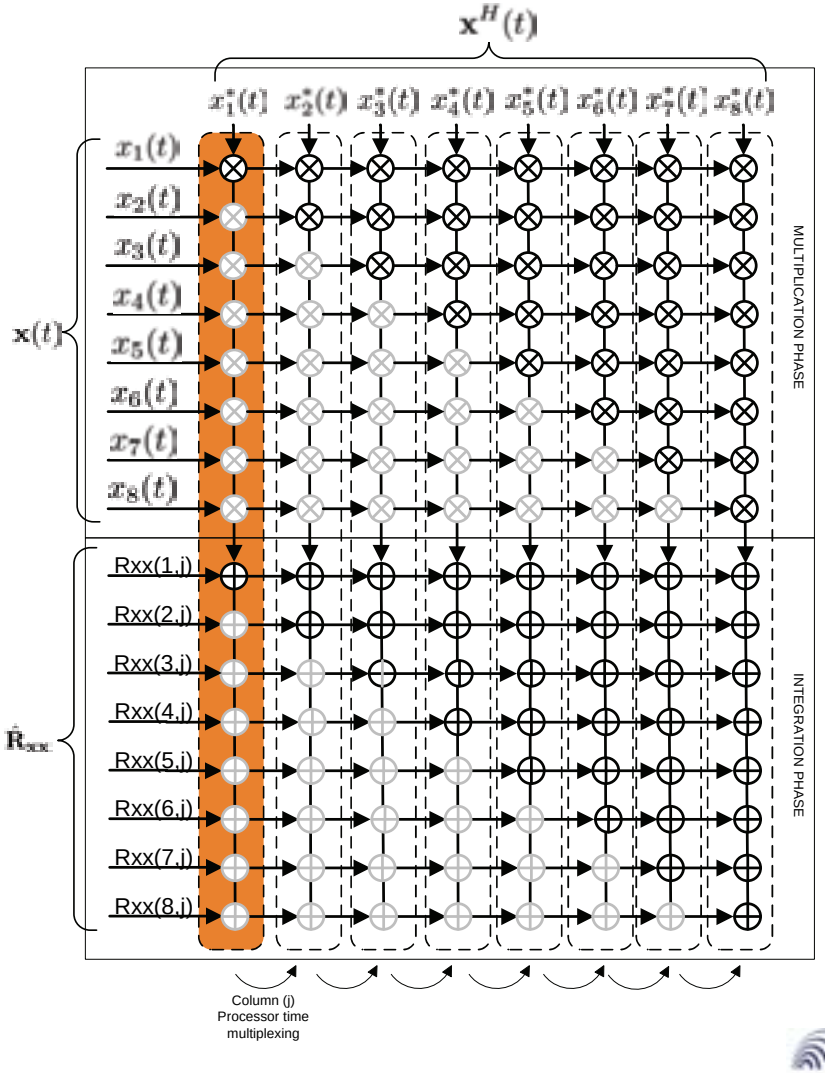

Real-time logic for $\hat{\mathbf{R}}_{\mathbf{xx}}$.

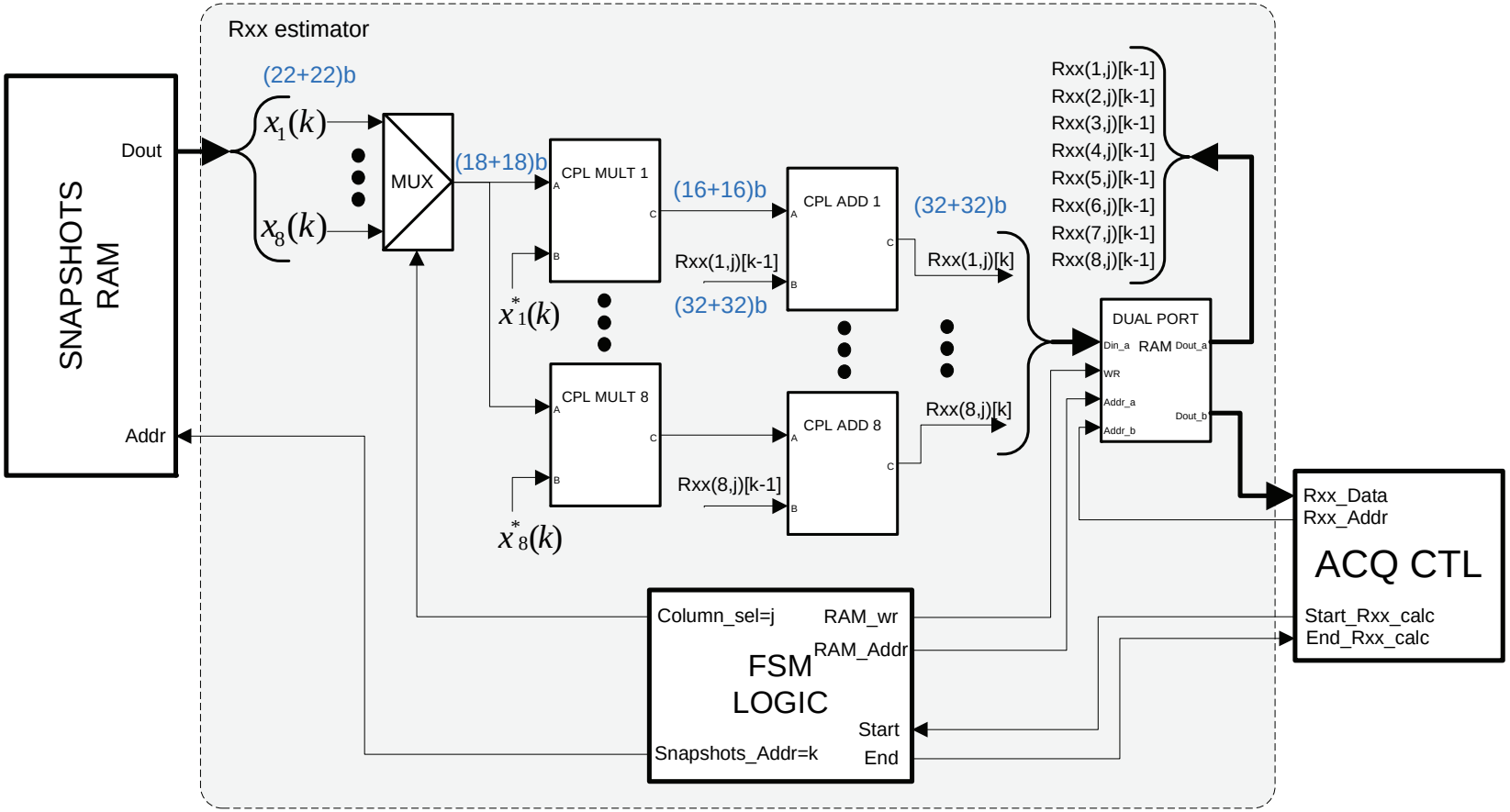

Cross-correlation vector estimation implementation

$$\hat{\mathbf{r}}_{\mathbf{xd}}(\check{f}_d, \check{\boldsymbol{\tau}}) = \frac{1}{K}\mathbf{X}\mathbf{d}(\check{f}_d, \check{\tau})^H =$$

$$= \left[\sum_{k=1}^{K} x_1(k) e^{-j2\pi \check{f}_d} d^*(k, \check{\tau}), \ \ldots, \sum_{k=1}^{K} x_N(k) e^{-j2\pi \check{f}_d} d^*(k, \check{\tau}) \right]. \qquad (36)$$

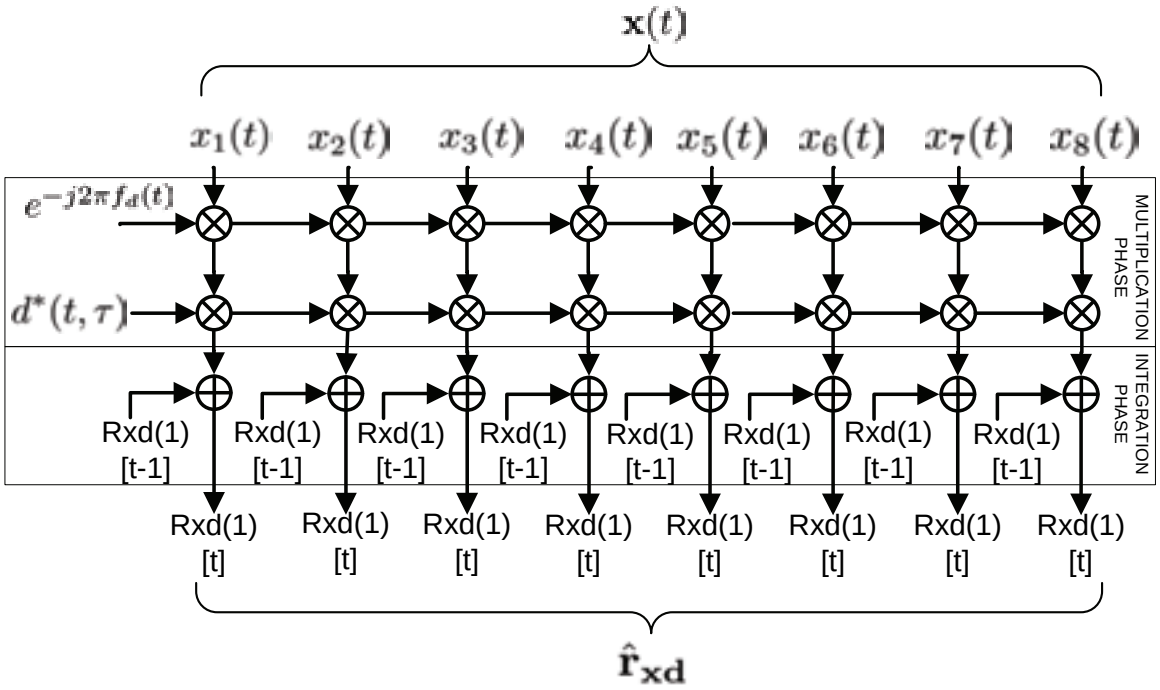

Real-time logic for $\hat{\mathbf{r}}_{\mathbf{xd}}$.

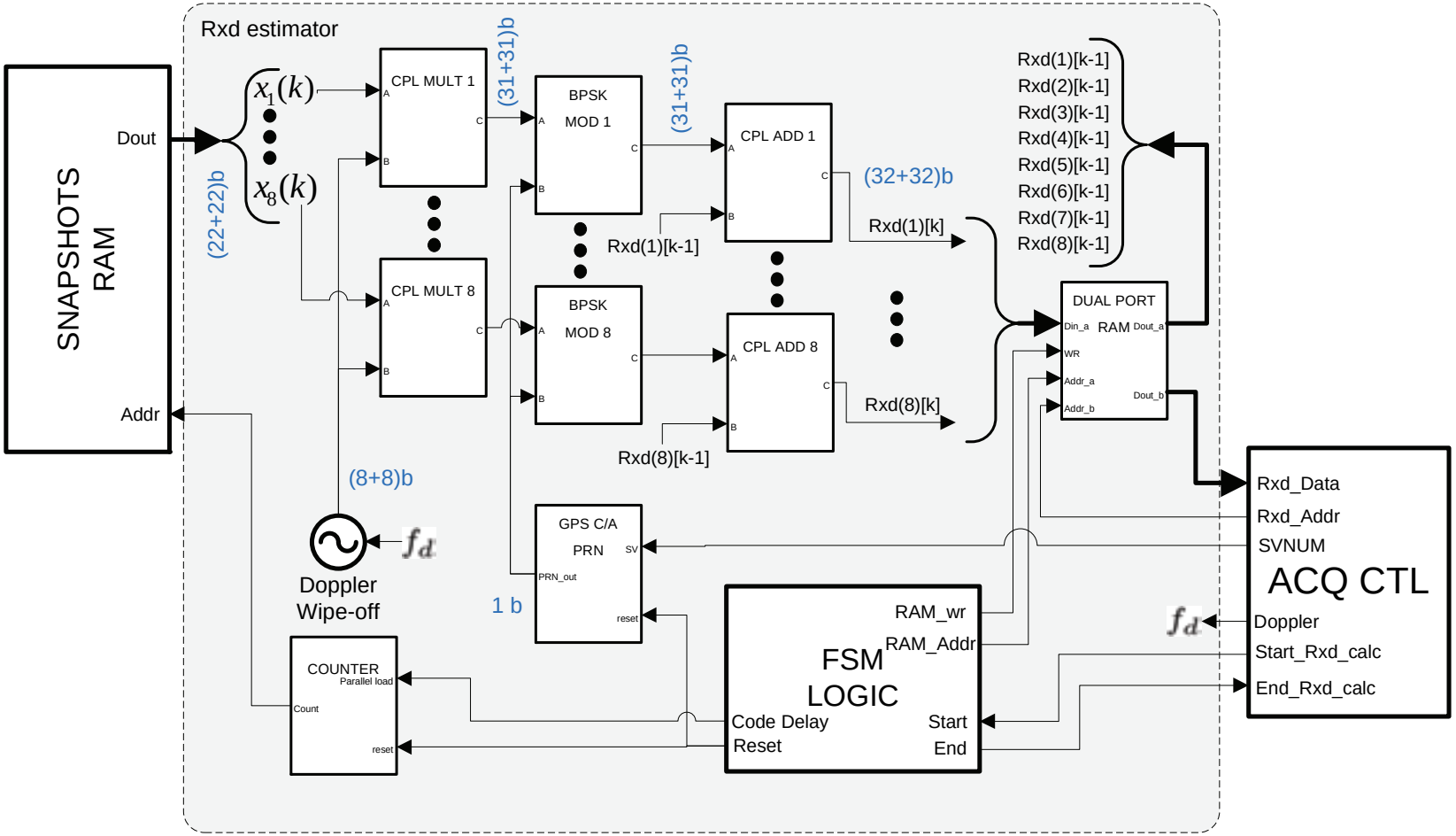

High-level operations: FPGA embedded software-defined processor

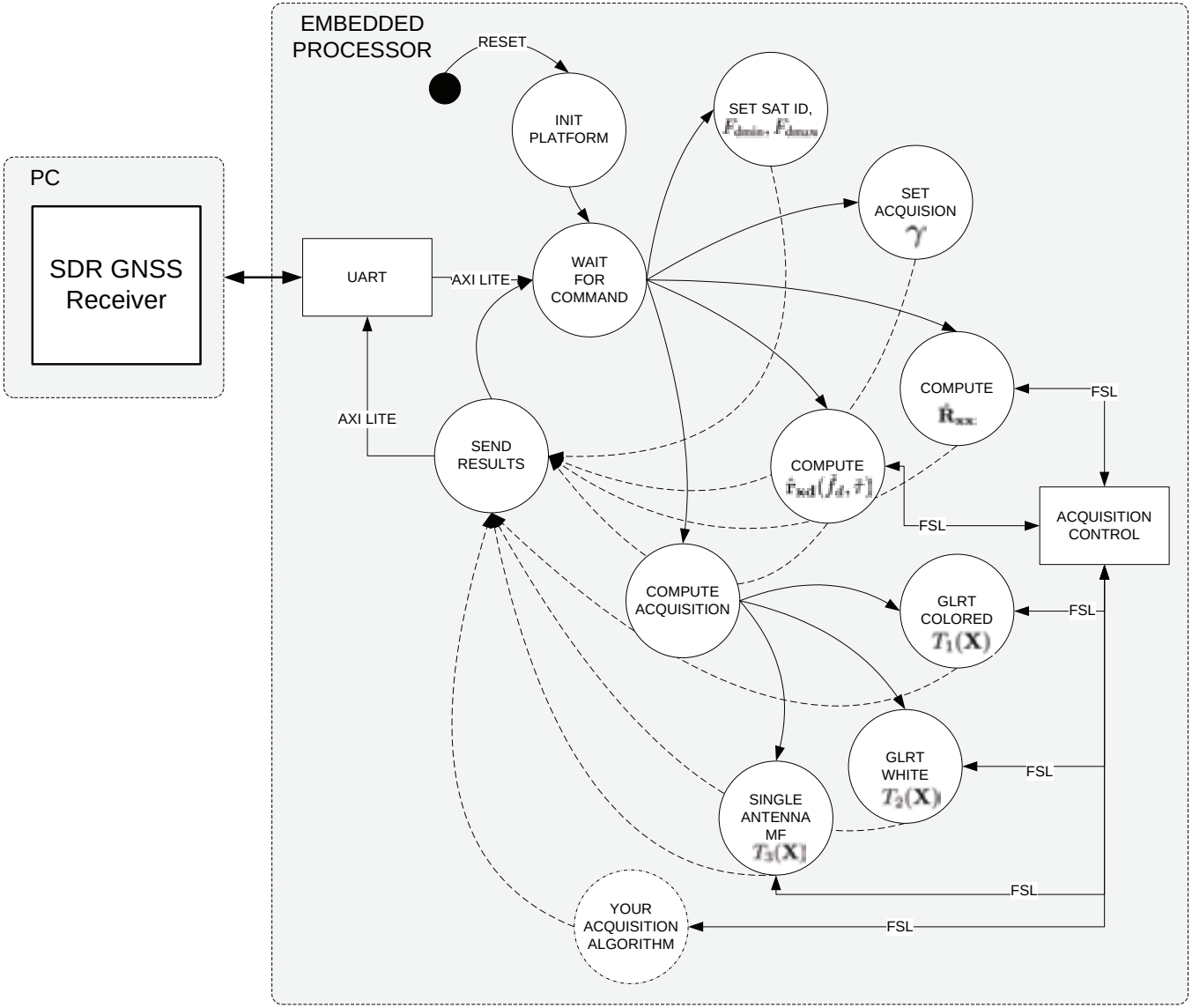

Calibration process

1. **Generate a reference carrier** $f_{\text{cal}} = f_c + f_{\text{ref}}$, capture $\mathbf{X}$, and **estimate the amplitudes** vector $\mathbf{a}_{\text{cal}} = [\frac{1}{\sqrt{\hat{P}_1}}, \ldots, \frac{1}{\sqrt{\hat{P}_N}}] \in \mathbb{R}^{1\times N}$, where $\hat{P}_i = \frac{1}{K}\sum_0^{K-1} x_i x_i^*$
2. **Estimate the phase shifts** between the reference channel and rest of the channels using the ML estimator and compute $\phi_{\text{cal}} = \left[e^{-j2\pi\frac{\Delta\hat{k}_1 f_{\text{ref}}}{f_s}}, \ldots, e^{-j2\pi\frac{\Delta\hat{k}_i f_{\text{ref}}}{f_s}}\right] \in \mathbb{C}^{1\times N}$.
3. **Compute** $\mathbf{G}_{\text{cal}} = \text{diag}(\mathbf{a}_{\text{cal}})\,\text{diag}(\phi_{\text{cal}})$ and **apply it to the snapshots** as $\mathbf{X}_{\text{cal}} = \mathbf{G}_{\text{cal}}\mathbf{X}$.

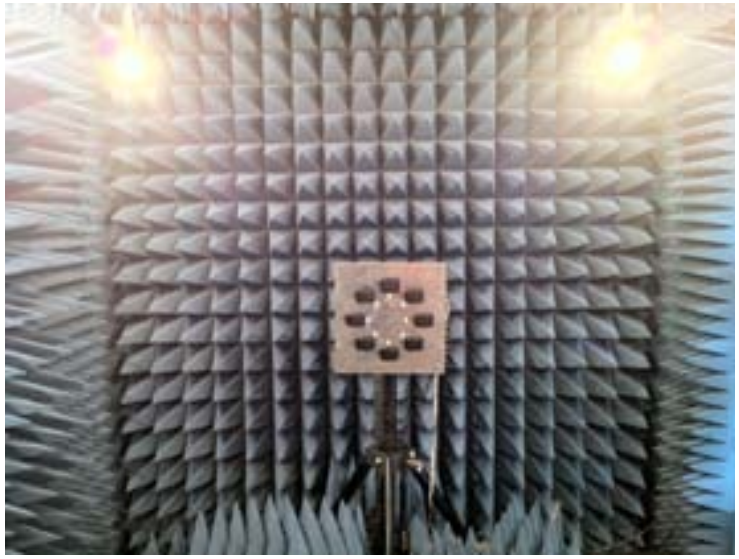

Figure: Calibration setup in an anechoic chamber.

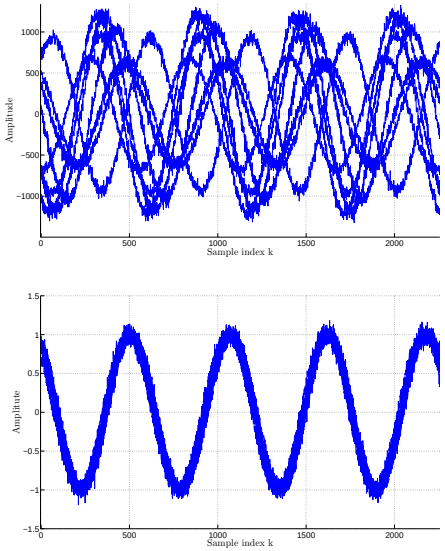

Figure: Uncalibrated and calibrated snapshots plots for $f_{\text{ref}} = 10$ kHz.

Calibration validation I

A spectral Multiple Signal Classification (MUSIC) algorithm was used to **estimate a test signal DOA and verify the array calibration**:

$$(\hat{\theta}, \hat{\psi}) = \arg\max_{\theta,\psi} \frac{1}{\mathbf{v}(\theta,\psi)^H(\mathbf{I} - \mathbf{u}\mathbf{u}^H)\mathbf{v}(\theta,\psi)}, \tag{37}$$

where $\mathbf{v}(\theta,\psi) \in \mathbb{C}^{N\times 1}$ is the signal steering vector, $\mathbf{u} \in \mathbb{C}^{N\times 1}$ is the eigenvector associated with the most powerful eigenvalue of $\hat{\mathbf{R}}_{\mathbf{xx}}$, and $\mathbf{I} \in \mathbb{R}^{N\times N}$ is the identity.

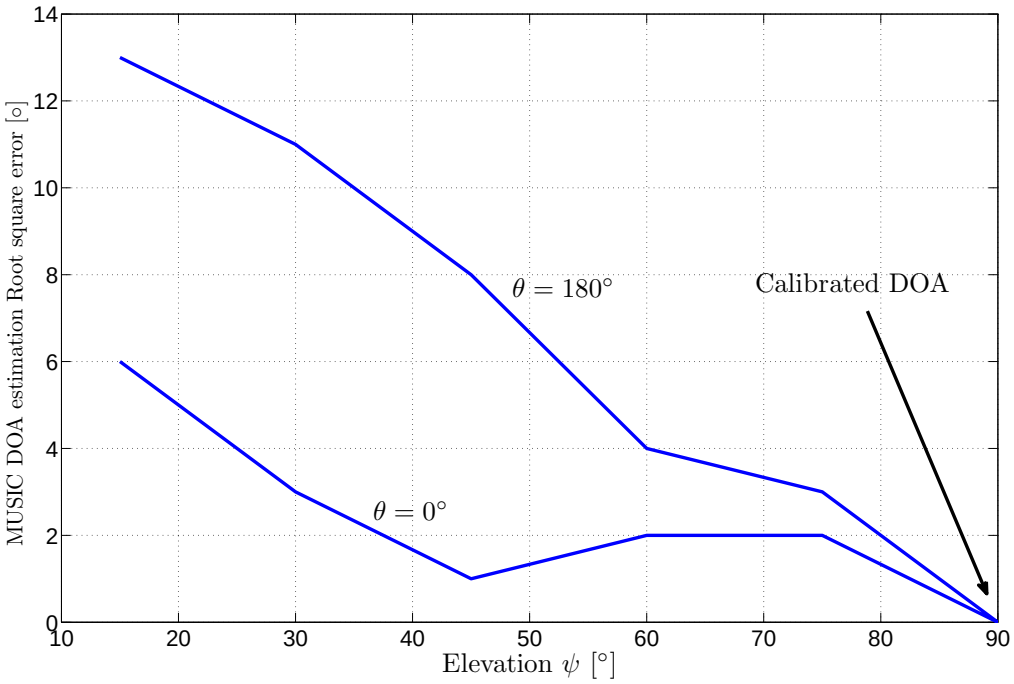

Figure: DOA elevation estimation pointing error for $\theta = 0°$ and $\theta = 180°$ (**The array was calibrated in the broadside direction $\psi = 90°$**).

Calibration validation II

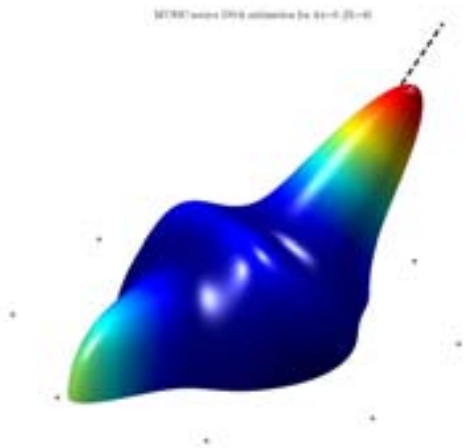

Figure: MUSIC signal DOA estimation for $\theta = 0°$, $\psi = 45°$.

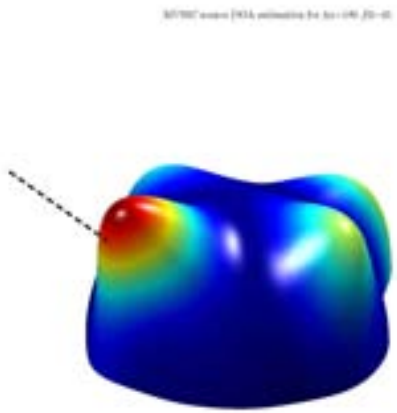

Figure: MUSIC signal DOA estimation for $\theta = 180°$, $\psi = 45°$.

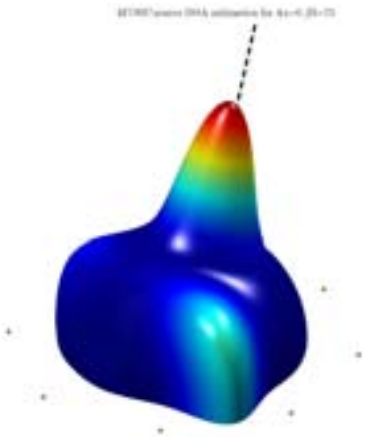

Figure: MUSIC signal DOA estimation for $\theta = 0°$, $\psi = 75°$.

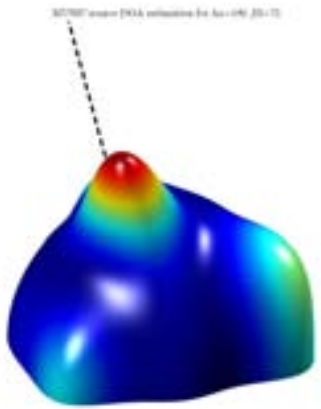

Figure: MUSIC signal DOA estimation for $\theta = 180°$, $\psi = 75°$.

Interference scenario setup

- A GPS L1 C/A satellite signal is transmitted using a horn antenna, with $\theta = 0°$ and $\psi = 90°$, **simulating a realistic situation were a high elevation satellite is received** with $C/N_0 = 44$ dB-Hz.
- An interference signal is transmitted using an auxiliary monopole antenna with an approximated DOA of $\theta = 45°$ and $\psi = 45°$, which **simulates a moderate elevation jammer or a communication signal coming from nearby communication tower**.
- The interference signal and the satellite signal were generated by two Agilent E4438C generators. The latter was equipped with GPS Personality.
- The test functions were executed using $T_{\text{acq}} = 1$ ms of captured snapshots.

Interference scenario setup

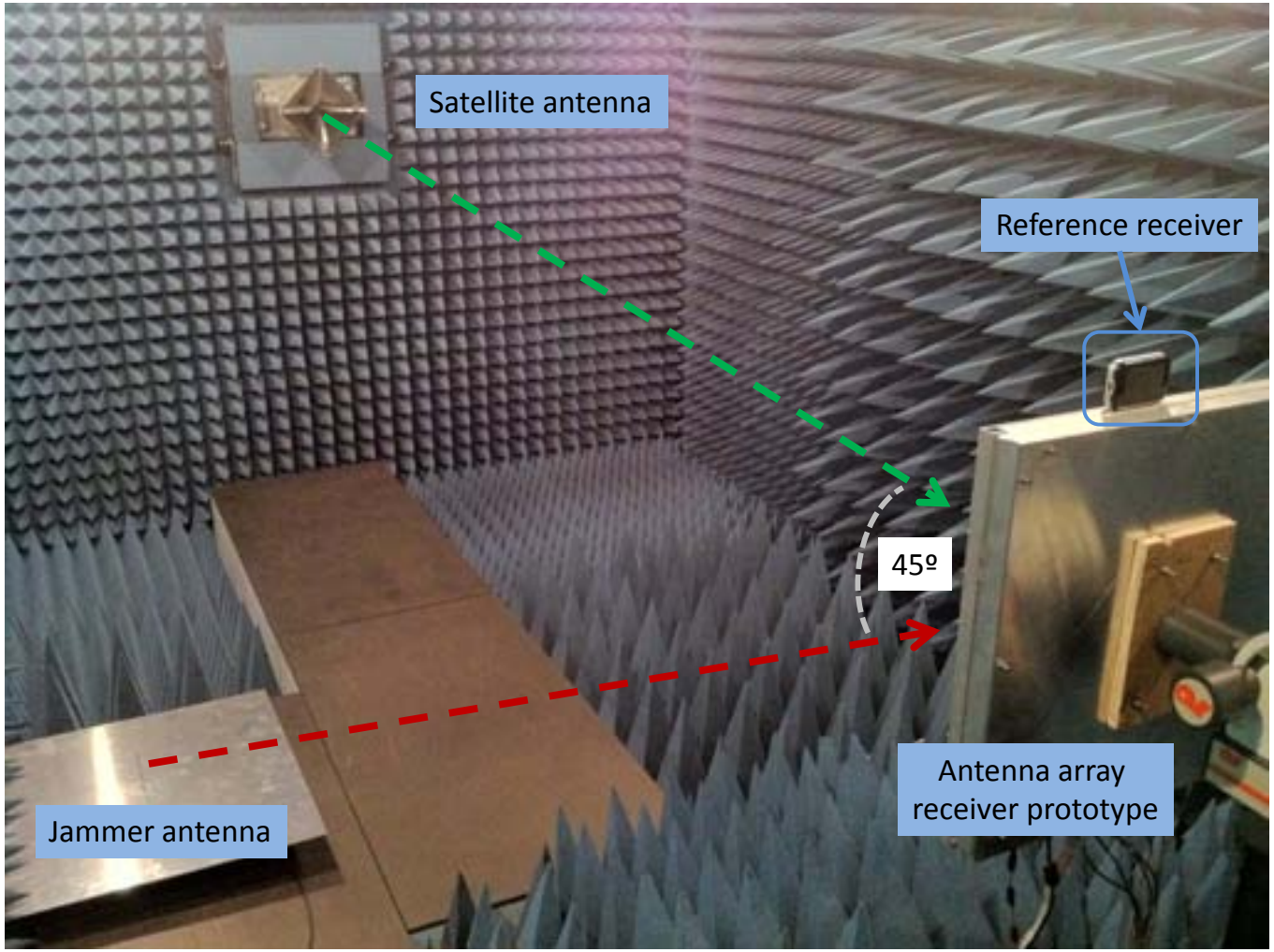

Implemented acquisition functions

- **GLRT colored**

$$T_1(\mathbf{X}) = \max_{f_d,\tau} \left\{ \hat{\mathbf{r}}_{\mathbf{xd}}^H(f_d,\tau)\hat{R}_{\mathbf{dd}}^{-1}\hat{\mathbf{R}}_{\mathbf{xx}}^{-1}\hat{\mathbf{r}}_{\mathbf{xd}}(f_d,\tau) \right\} > \gamma. \tag{38}$$

- **GLRT white**

$$T_2(\mathbf{X}) = \max_{f_d,\tau} \left\{ \frac{\hat{\mathbf{r}}_{\mathbf{xd}}(f_d,\tau)^H\hat{\mathbf{r}}_{\mathbf{xd}}(f_d,\tau)}{\mathrm{Tr}(\hat{\mathbf{R}}_{\mathbf{xx}})} \right\} > \gamma. \tag{39}$$

- **Single antenna MF**

$$T_3(\mathbf{X},i) = \max_{f_d,\tau} \left\{ \sum_{t=0}^{K-1} \|x_i(t)e^{-j2\pi f_d}d^*(t,\tau)\|^2 \right\} > \gamma, \tag{40}$$

where i is the selected antenna element.

Acquisition results for CW interference

A **Continuous Wave (CW) jammer** impinges into the array with $f_{\text{int}} = 1575.43$ MHz and $J/N_0 = 133$ dB-Hz.

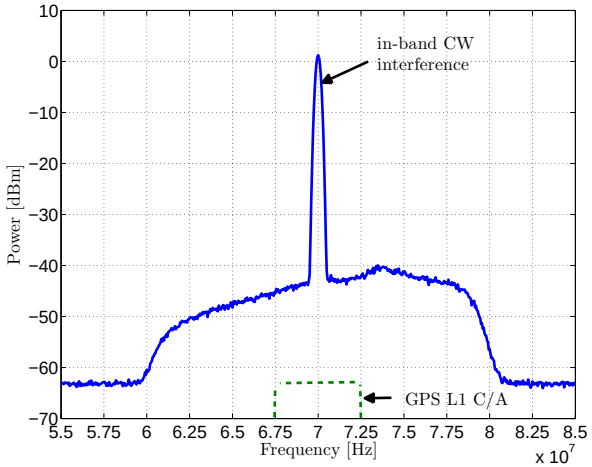

(a) IF spectrum.

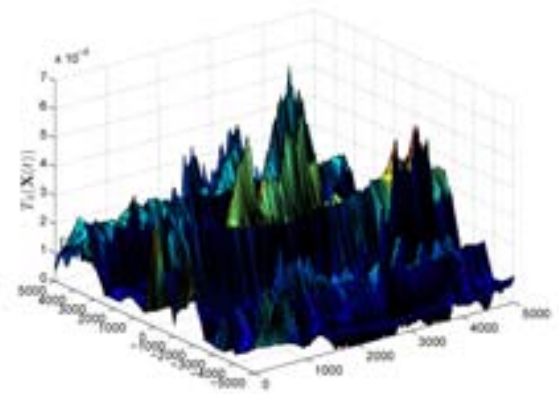

(b) $T_{\text{Single}}(\mathbf{x}(t,\check{f}_d,\check{\tau}))$.

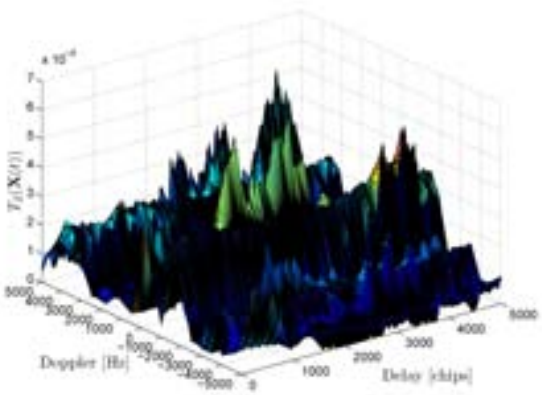

(c) $T_{\text{GL White}}(\mathbf{X}(t,\check{f}_d,\check{\tau}))$.

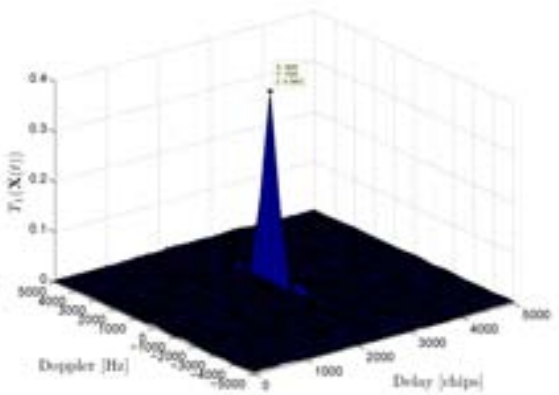

(d) $T_{\text{GL Colored}}(\mathbf{X}(t,\check{f}_d,\check{\tau}))$.

Acquisition results for 4G/LTE

A possible **Lightsquared interference** was simulated using a Long Term Evolution (LTE) downlink signal with 5 MHz of bandwidth, impinging into the array with $f_{\text{int}} = 1575.42$ MHz and $J/N_0 = 133$ dB-Hz.

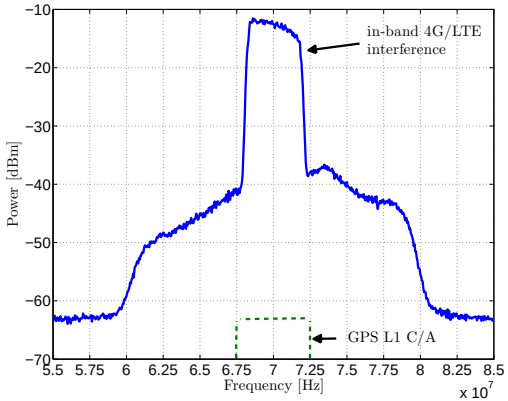

(e) IF spectrum.

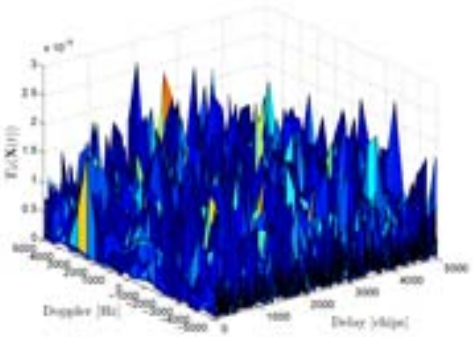

(f) $T_{\text{Single}}(t, \check{f}_d, \check{\tau}))$.

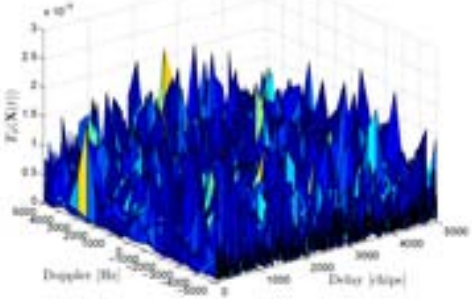

(g) $T_{\text{GL White}}(t, \check{f}_d, \check{\tau}))$.

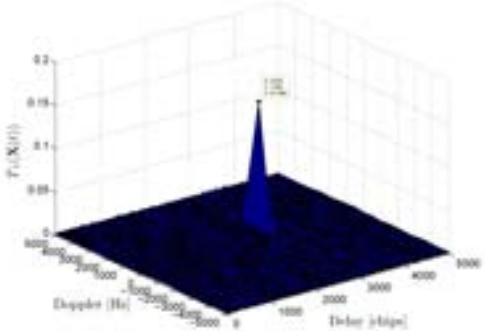

(h) $T_{\text{GL Colored}}(t, \check{f}_d, \check{\tau}))$.

Deflection coefficient

The deflection coefficient is defined as

$$d^2 = \frac{(\mathbb{E}\{T(\mathbf{X};\mathcal{H}_1)\} - \mathbb{E}\{T(\mathbf{X};\mathcal{H}_0)\})^2}{\mathrm{var}\{T(\mathbf{X};\mathcal{H}_0)\}}. \tag{41}$$

In the measurements, the expectations operators and the variance operator were substituted by its sample mean and sample variance respectively.

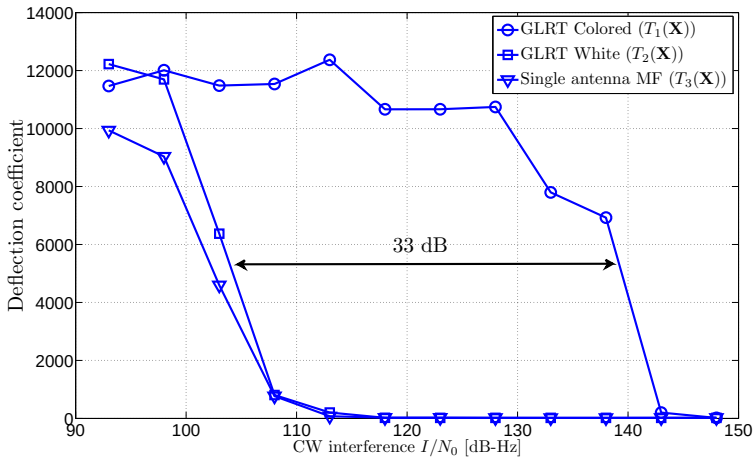

(i) CW interference scenario.

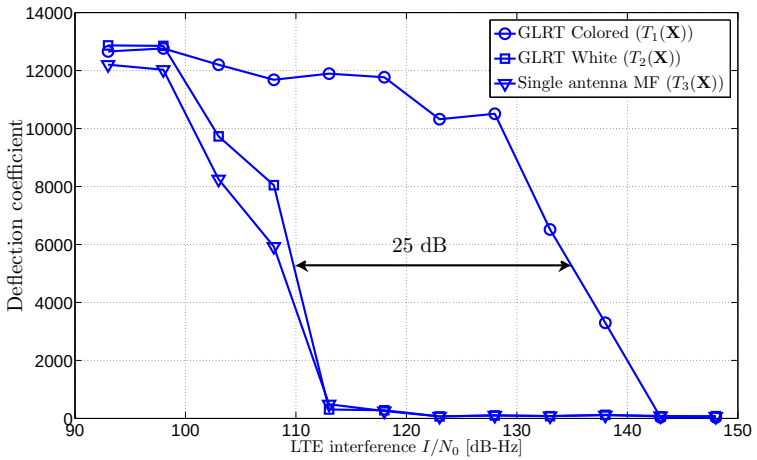

(j) LTE interference scenario.

Theoretical analysis

Done:

- ✓ **GLRT extension to the GNSS array signal model** assuming an **arbitrary and unknown covariance noise matrix**. The obtained detector is able to **mitigate temporally uncorrelated interferences** even if the array is **unstructured** and moderately **uncalibrated**.
- ✓ The performance and the interference rejection capability were modeled and compared to their theoretical bound. The detector was proven to be a **UMP test detector and has CFAR properties**.
- ✓ The proposed acquisition algorithm was compared to conventional acquisition after the MVDR beamformer. The **MVDR is severely affected by moderate pointing errors and/or array miss-calibration, while the GLRT detector remains insensible to this situation**.
- ✓ **Analysis of realistic conditions** to obtain preliminary **hardware requirements** for an implementation of the algorithm.
- ✓ The effect of the signal bandwidth in the acquisition has been modeled: **an increase of the bandwidth beyond the main spectrum lobe reduces the SNR, and, consequently, reduces also the performance of the acquisition** algorithms.

Theoretical analysis

To Do:

- Explore the application of the **Bayesian approach** to the acquisition problem; it might be possible to **estimate a prior PDF for the synchronization parameters** and integrate them in the GLRT detector.
- Integration of **inertial sensors** in the receiver at acquisition stage.
- Ultimately, an **hybridization between array-based acquisition and tracking** might be possible, since both algorithms are related in the sense that acquisition contains prior information suitable for tracking initialization and vice-versa.

Design and implementation of a real-time array-based GNSS receiver platform

Done:

- ✓ **A novel real-time array-based GNSS receiver platform was developed**:
  - ✓ A complete signal reception chain, including the antenna array and the multichannel RF front-end for the GPS L1/ Galileo E1 was designed, implemented and tested.
  - ✓ The **FPGA** digital processing section of the platform, such as the array signal statistics extraction modules were also implemented.
  - ✓ Coupled with a software defined receiver.
- ✓ Design trade-offs and implementation complexities were carefully analyzed and taken into account.
- ✓ **Proof-of-concept prototype**: the array-based acquisition algorithm introduced in this Dissertation was implemented and tested under realistic conditions.
- ✓ **Harsh in-band interference scenarios were tested**, including narrow/wide band interferers and communication signals. **The performance results were aligned with the theoretical and simulated ones**, thus, completing the algorithm validation.

Design and implementation of a real-time array-based GNSS receiver platform

To Do:

- The platform can be enhanced by **integrating an IMU**.
- Design and implementation of **dual-band antenna elements patches** to cover both the GPS L1 / Galileo E1 and the GPS L5 Galileo E5a links, which provide a complete SoL signals coverage of two of the most evolved GNSS.
- Explore the **integration of array elements and front-end calibration procedures**.
- Explore the application of **open source soft processors** such as the Aeroflex Gaisler LEON3 to replace the Microblaze implementation. Ultimately, it should be possible to **integrate the GNU Radio framework and the GNSS-SDR software receiver in the soft processor**.

Interference mitigation in GNSS signal acquisition through antenna arrays

Dr. Javier Arribas
(jarribas@cttc.es)

Interference Management for Tomorrow's Wireless Networks

Newcom# Summer School Sophia Antipolis - May 28-31, 2013

Thank you for your attention!

Existing solutions: Acquisition after beamforming

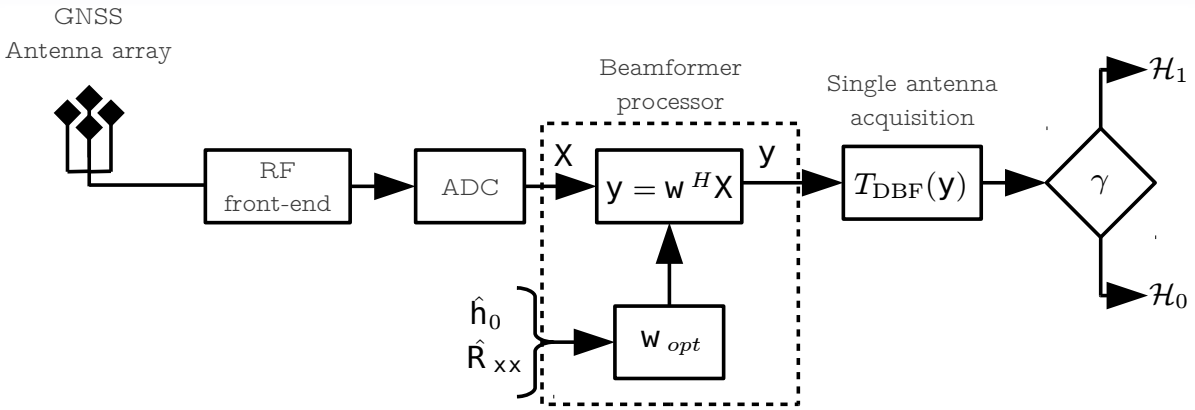

Figure: Acquisition after beamforming concept.

Beamformer output signal model and GLRT test function:

$$\mathbf{y} = \mathbf{w}^H \mathbf{X}, \tag{42}$$

$$T_{\mathrm{DBF}}(\mathbf{X}) = \max_{f_d,\tau} \frac{\hat{R}^H_{\mathbf{yd}}(f_d,\tau)\hat{R}_{\mathbf{yd}}(f_d,\tau)}{\hat{R}_{\mathbf{yy}}} > \gamma, \tag{43}$$

where $\mathbf{w} \in \mathbb{C}^{N\times 1}$ is the beamformer weights vector, and

$$\hat{R}_{\mathbf{yd}} = \frac{1}{K}\mathbf{y}\mathbf{d}^H = \mathbf{w}^H \frac{1}{K}\mathbf{X}\mathbf{d}^H = \mathbf{w}^H \hat{\mathbf{r}}_{\mathbf{xd}} \tag{44}$$

$$\hat{R}_{\mathbf{yy}} = \frac{1}{K}\mathbf{y}\mathbf{y}^H = \mathbf{w}^H \hat{\mathbf{R}}_{\mathbf{xx}}\mathbf{w}. \tag{45}$$

Existing solutions: Acquisition after beamforming

Test function distribution

$$T_{\mathrm{DBF}}(\mathbf{X}) \sim \begin{cases} \chi_2^2(\delta_{T_{\mathrm{DBF}};\mathcal{H}_1}), & \text{in } \mathcal{H}_1, \\ \chi_2^2(\delta_{T_{\mathrm{DBF}};\mathcal{H}_0} = 0), & \text{in } \mathcal{H}_0, \end{cases} \tag{46}$$

where $\sigma^2_{T_{\mathrm{DBF}}} = \frac{1}{2K}$ and

$$\delta_{T_{\mathrm{DBF}};\mathcal{H}_1} = \frac{\|\mu_{\hat{R}_{\mathbf{yd}}}\|^2}{\hat{R}_{\mathbf{yy}}} = \frac{\mathbf{w}^H R_{\mathbf{dd}} \mathbf{h}\mathbf{h}^H R^*_{\mathbf{dd}} \mathbf{w}}{\mathbf{w}^H \mathbf{R}_{\mathbf{xx}} \mathbf{w}}. \tag{47}$$

Performance expressions

$$P_d(\gamma) = \mathrm{Q}_1\left(\frac{\sqrt{\delta_{T_{\mathrm{DBF}};\mathcal{H}_1}}}{\sigma_{T_{\mathrm{DBF}}}}, \frac{\sqrt{\gamma}}{\sigma_{T_{\mathrm{DBF}}}}\right), \tag{48}$$

$$P_{fa}(\gamma) = \exp\left\{\frac{-\gamma}{2\sigma^2_{T_{\mathrm{DBF}}}}\right\}, \tag{49}$$

where Q_1 is the generalized Marcum Q-function of order 1. The acquisition test statistic is CFAR.

Existing solutions: MVDR beamformer

Minimum Variance Distortionless Response (MVDR) optimum weights

$$\begin{aligned} &\min_{\mathbf{w}} \mathbf{w}^H \mathbf{R}_{\mathbf{xx}} \mathbf{w} \\ &\text{s.t } \mathbf{w}^H \mathbf{h}_0 = 1, \end{aligned} \tag{50}$$

where $\mathbf{h}_0 \in \mathbb{C}^{N\times 1}$ is the **DOA steering vector**. Then,

$$\mathbf{w}_{\text{opt}} = \frac{\mathbf{R}_{\mathbf{xx}}^{-1}\mathbf{h}_0}{\mathbf{h}_0^H \mathbf{R}_{\mathbf{xx}}^{-1}\mathbf{h}_0}. \tag{51}$$

MVDR GLRT test function

$$T_{\text{MVDR}}(\mathbf{X}) = \frac{\hat{\mathbf{r}}_{\mathbf{xd}}^H (\mathbf{R}_{\mathbf{xx}}^{-1}\mathbf{h}_0)(\mathbf{R}_{\mathbf{xx}}^{-1}\mathbf{h}_0)^H \hat{\mathbf{r}}_{\mathbf{xd}}}{\mathbf{h}_0^H \mathbf{R}_{\mathbf{xx}}^{-1}\mathbf{h}_0} \simeq \frac{1}{\sigma^2} \frac{|\hat{\mathbf{r}}_{\mathbf{xd}}^H \mathbf{P}_{\mathbf{H}_i}^{\perp} \mathbf{h}_0|^2}{\|\mathbf{h}_0^H \mathbf{P}_{\mathbf{H}_i}^{\perp}\|^2}. \tag{52}$$

Existing solutions: Power minimization beamformer

Design condition: the **DOA is unavailable**. The beamformer minimizes the output power while not weighting a reference antenna ($\mathbf{h}_0 = [1\,0\ldots0]$).

Performance in absence of interferences ($\mathbf{P}^{\perp}_{\mathbf{H}_i} = \mathbf{I}$)

$$T_{\mathrm{PWR}}(\mathbf{X}) = \sigma^{-2}\|\mathbf{r}^H_{\mathbf{xd}}\mathbf{h}_0\|^2 = T_{\mathrm{GL}}(\mathbf{x}_1, f_d, \tau). \tag{53}$$

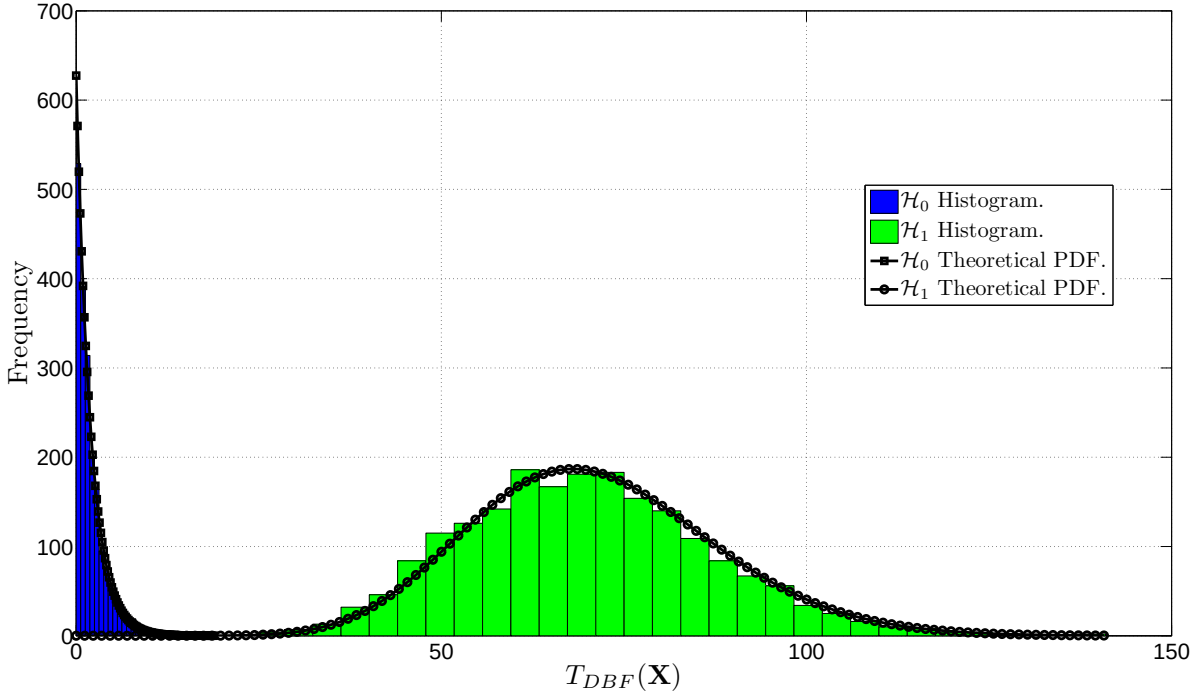

Figure: $T_{\mathrm{PWR}}(\mathbf{X})$ histogram and theoretical PDF in both $\mathcal{H}_1$ and $\mathcal{H}_0$ acquisition hypotheses for Galileo E1 signal acquisition simulation.

J. Arribas, *GNSS Array-based Acquisition: Theory and Implementation*, PhD Thesis, Universitat Politècnica de Catalunya (UPC), Barcelona, Spain, June 2012.

C. Fernández-Prades, *Advanced Signal Processing Techniques for GNSS Receivers*, PhD Thesis, Universitat Politècnica de Catalunya (UPC), Barcelona, Spain, May 2006.

B.W. Parkinson, and J.J. Spilker (eds.), *Global Positioning System: Theory and Applications, vol. I, II*, Progress in Astronautics and Aeronautics, American Institute of Aeronautics, Inc., Washington DC, 1996.

L. Weill, "C/A Code Pseudoranging Accuracy-How Good Can it Get?", *Proceedings of ION GPS-94, the 7th International Technical Meeting of the Satellite Division of the Institute of Navigation*, pp. 133–141, Salt Lake City, UT, 1994.

J. R. Williams, "U.S. Spectrum Allocations 300 - 3000 MHz", Tech. rep., OPP/FCC, 2002.